

RESEARCH ARTICLE

TREK-1 channels regulate pressure sensitivity and calcium signaling in trabecular meshwork cells

Oleg Yarishkin¹ , Tam T.T. Phuong¹, Colin A. Bretz¹ , Kenneth W. Olsen¹ , Jackson M. Baumann^{1,2,3}, Monika Lakk¹, Alan Crandall¹, Catherine Heurteaux⁴, Mary E. Hartnett¹, and David Krizaj^{1,2,3,5} 

Mechanotransduction by the trabecular meshwork (TM) is an essential component of intraocular pressure regulation in the vertebrate eye. This process is compromised in glaucoma but is poorly understood. In this study, we identify transient receptor potential vanilloid isoform 4 (TRPV4) and TWIK-related potassium channel-1 (TREK-1) as key molecular determinants of TM membrane potential, pressure sensitivity, calcium homeostasis, and transcellular permeability. We show that resting membrane potential in human TM cells is unaffected by “classical” inhibitors of voltage-activated, calcium-activated, and inwardly rectifying potassium channels but is depolarized by blockers of tandem-pore K⁺ channels. Using gene profiling, we reveal the presence of TREK-1, TASK-1, TWIK-2, and THIK transcripts in TM cells. Pressure stimuli, arachidonic acid, and TREK-1 activators hyperpolarize these cells, effects that are antagonized by quinine, amlodipine, spadin, and short-hairpin RNA-mediated knockdown of TREK-1 but not TASK-1. Activation and inhibition of TREK-1 modulates [Ca²⁺]_{TM} and lowers the impedance of cell monolayers. Together, these results suggest that tensile homeostasis in the TM may be regulated by balanced, pressure-dependent activation of TRPV4 and TREK-1 mechanotransducers.

Introduction

Intraocular pressure (IOP) is the most significant risk factor for glaucoma (Kass et al., 2002; Leske et al., 2003), with current treatment largely limited to IOP-lowering agents that target the secretion of aqueous humor from the ciliary body or its drainage through the pressure-insensitive “uveoscleral” pathway. However, by far the largest outflow component (~90%) in the primate eye is mediated by the trabecular meshwork (TM), which filters and funnels aqueous humor into the canal of Schlemm (Lütjen-Drecoll and Rohen, 1989). Unlike the ciliary body and muscle, this conventional TM pathway is mechanosensitive and protects the eye from hypertension by autoregulating fluid outflow under different pressure regimens (Brubaker, 1975; Lei et al., 2011). The trabecular outflow mechanism is often compromised in glaucoma, as TM cells adopt the properties of contractile myofibroblasts that chronically augment the tissue resistance to fluid outflow (Flügel et al., 1991; Last et al., 2011). Given that TM has remained intractable to antiglaucoma medications, understanding how its cells sense and transduce pressure is a matter of considerable academic and clinical interest.

We recently identified the nonselective cation channel TRPV4 as a cell volume sensor (Toft-Bertelsen et al., 2017) and likely TM transducer of pressure, swelling, and strain (Ryskamp et al., 2016). In vitro and in vivo experiments revealed that TRPV4 plays a central role in Ca²⁺-dependent cytoskeletal up-regulation, TM resistance to fluid outflow, and regulation of IOP. TRPV4 antagonists lowered IOP in chronically hypertensive eyes but had no effect on healthy eyes (Jo et al., 2016; Ryskamp et al., 2016), suggesting that steady-state tensile homeostasis and mechanoadaptation in TM cells rely on additional mechanosensing mechanisms. In this study, we investigated the background pressure dependence in human TM cells using electrophysiology, pharmacology, RNA silencing, and impedance measurements. We demonstrate that TREK-1, a polymodal mechanosensitive tandem-pore potassium (K_{2P}) channel (Meadows et al., 2000), represents a crucial molecular link between the membrane potential of primary and immortalized TM cells and their sensitivity to pressure. TREK-1 is activated by multiple types of mechanical force (strain, swelling, shear flow, and stretch) and functions as a regulator of mechanical thresholds, nociception, and stretch-in-

¹Department of Ophthalmology & Visual Sciences, University of Utah School of Medicine, Salt Lake City, UT; ²Department of Bioengineering, University of Utah School of Medicine, Salt Lake City, UT; ³Bioengineering Graduate Program, University of Utah School of Medicine, Salt Lake City, UT; ⁴Institute de Pharmacologie Moléculaire et Cellulaire, CNRS, Valbonne, France; ⁵Department of Neurobiology & Anatomy, University of Utah School of Medicine, Salt Lake City, UT.

Correspondence to David Krizaj: david.krizaj@hsc.utah.edu; Oleg Yarishkin: yarishkin@gmail.com.

Part of this work was presented at the Association for Retinal and Visual Science meeting held in Honolulu, HI, April 29–May 3, 2018, and has appeared in abstract form (Yarishkin et al., 2018).

© 2018 Yarishkin et al. This article is distributed under the terms of an Attribution–Noncommercial–Share Alike–No Mirror Sites license for the first six months after the publication date (see <http://www.rupress.org/terms/>). After six months it is available under a Creative Commons License (Attribution–Noncommercial–Share Alike 4.0 International license, as described at <https://creativecommons.org/licenses/by-nc-sa/4.0/>).

duced contractility in neurons, bladder, colon, and uterine cells (Patel et al., 1999; Talley et al., 2001; Gruss et al., 2004; Heurteaux et al., 2004; Alloui et al., 2006; Nayak et al., 2009; Baker et al., 2010; Monaghan et al., 2011; Noël et al., 2011). Its sensitivity to temperature, pH, long-chain polyunsaturated fatty acids (such as arachidonic acid [AA]), and widely used anesthetics, antidepressants, and neuroleptics (Enyedi and Czirják, 2010; Brohawn et al., 2014; Feliciangeli et al., 2015) allows these channels to integrate the cells' electrical properties with mechanotransduction to tune a wide spectrum of ambient signals. TRPV4 and TREK-1 channels were reported to regulate the TM cytoskeleton and were implicated in glaucoma (Ryskamp et al., 2016; Carreon et al., 2017), yet it is unclear whether they can be activated by physiologically relevant pressures and how they collaborate in pressure transduction. Here, we characterize the response of TREK-1 to pressure steps and AA and delineate its function as a gatekeeper for Ca²⁺ homeostasis and ECM adhesion. We show that the TM pressure response involves opposing activation of TRPV4 and TREK-1, which cooperate in control of pressure-dependent signaling, calcium homeostasis, and cell–ECM interactions. These findings place TREK-1 in the center of mammalian IOP regulation, and therefore vision, and suggest a novel mechanism for pressure dysregulation in open-angle glaucoma.

Materials and methods

Cell culture and transfection

Immortalized cells, isolated from the juxtacanalicular region of the human eye (hTM cells), were purchased from ScienCell Research Laboratories. Key physiological features (e.g., TREK-1 dependence of the membrane potential) were also tested in primary TM cells (pTM cells) isolated from corneal rims from three donors (aged between 35 and 60 yr) with no history of eye disease. The rims were acquired and used in concordance with the tenets of the WMA Declaration of Helsinki and the Department of Health and Human Services Belmont Report. The identity of TM cells was validated as described (Ryskamp et al., 2016; Stamer and Clark, 2017), with hTM/pTM exhibiting similar genetic/biochemical/molecular signatures (expression of TM-specific markers, smooth muscle actin, and DEX-induced up-regulation of myocilin), responsiveness to ambient stimuli, and expression of K_{2P} and TRP channel transcripts. Cell cultures were maintained in the Trabecular Meshwork Cell Medium (ScienCell, 6591) at 37°C and 5% CO₂ and studied at passages 1–10 and 1–3, respectively. For some experiments, cells were transiently transfected with GFP-tagged short hairpin RNA (shRNA) constructs targeting human TREK-1, TASK-1, or scrambled shRNA (shTREK-1, shTASK-1, and scRNA, respectively), using Lipofectamine 3000 according to the manufacturer's (Thermo Fisher Scientific) instructions. The transfected cells showed no obvious changes in morphology, confluence, and viability and were used for experiments at the second to third day after transfection.

Reverse transcription (RT)-PCR assay

RNA was isolated as described (Ryskamp et al., 2016). Total RNA was extracted with TRI-Reagent (Sigma) with 2 µg used for complementary DNA (XLT cDNA super mix kit; Quanta). Quantita-

tive RT-PCR was performed with Apex-Cyber Green on CFX96 Touch Real-Time PCR (Bio-Rad). PCR conditions were as follows: 95°C for 15 min; 95°C for 15 s, 60°C for 1 min, 40 cycles. The primer sequences and data are shown in Table 1 as mean value of 2^{-ΔΔCt} ± SEM.

Western blots

hTM/pTM cells were lysed in a buffer containing the standard protein inhibitor cocktail (Santa Cruz Biotechnology). Total protein was heat inactivated for 3 min at 95°C in Laemmli buffer (Bio-Rad). 30 µg total protein per lane was loaded in 8% mini polyacrylamide gels. Electrophoresis was performed at 90 V for 1 h in the Mini-PROTEAN Tetra apparatus (Bio-Rad; running buffer 25 mM Tris, 195 mM glycine, and 0.1% SDS). Proteins were transferred to a polyvinylidene fluoride membrane (0.2 µM, Bio-Rad) in transfer buffer (25 mM Tris, 195 mM glycine, and 20% methanol) in the Mini-PROTEAN Tetra apparatus at 4°C overnight. The membrane was blocked with 5% skim milk for 30 min, incubated overnight with anti-TREK-1 antibody (1:1,000, Santa Cruz Biotechnology) and anti-TASK-1 antibody (1:1,000, Alomone Labs), and washed with the TBS-T solution (TRIS-base [19 mM], NaCl [150 mM] and Tween-20 [0.1%] diluted in ddH₂O, pH 7.5) for 3 × 5 min each. Membranes were incubated with anti-rabbit HRP (1:2,000, Abcam) or GAPDH (1:5,000, Abcam) antibodies for 2 h at room temperature. Protein bands were detected on x-ray film by using enhanced chemiluminescence (Pierce) and developer (AFP Imaging Corp.).

Immunohistochemistry

Cells were plated on type I collagen-coated glass coverslips for 24 h and treated with DMSO (control group) or TREK-1 agonists for 1 h at 37°C. After fixation in 4% PFA, the cells were washed in PBS, permeabilized with 0.1% Triton X-100, and exposed to the blocking solution (1% BSA, 0.3% Triton X-100/PBS, and 0.1% Na₂S₂O₃).

Electrophysiology

Whole-cell recordings were conducted with borosilicate patch pipettes (tip resistance 6–7 MΩ). To avoid the potentially confounding contributions from intercellular junctions, the recordings were generally conducted in preconfluent cells with spindle-like morphology that is typical of metabolically active cells from the juxtacanalicular TM (Stamer and Clark, 2017). Whole-cell currents and the membrane potential were measured as described (Jo et al., 2016; Molnár et al., 2016) using a Multiclamp 700B amplifier, Digidata 1550 board, and Clampex 10.7 acquisition software (Molecular Devices). Cells were typically held at –30 mV, with current–voltage (I–V) relationships determined from voltage ramps imposed from –100 to 100 mV. Currents were sampled at 10 kHz, filtered at 5 kHz with an eight-pole Bessel filter, leak-subtracted after data acquisition, and analyzed with Clampfit 10.7 (Molecular Devices) and OriginPro 8 (Origin Lab). shRNA-transfected cells were recognized by GFP expression.

The external solution contained (in mM) 126 NaCl, 2.5 KCl, 1.5 MgCl₂, 1.5 CaCl₂, 1.25 NaH₂PO₄, 26 NaHCO₃, and 10 D-glucose (pH 7.4 was adjusted with NaOH). In some experiments, 5 mM NaCl was substituted with equimolar TEA-Cl. HEPES replaced

Table 1. **Primer list**

Name	Primer	Sequences (5'-3')	Amplicon (bp)	NCBI reference
TREK1	Forward	AGGGATTCTACTTGGCGGC	100	NM_001017424.2
	Reverse	CAAGCACTGTGGGTTTCGTG		
TREK2	Forward	CCTTCTCTGCTGCAAAGA	249	NM_138317.2
	Reverse	GATGCGATCCATCTGTCGT		
TASK1	Forward	CGCACTGGAGGTTCAAGCTA	311	NM_002246.2
	Reverse	CACCCCTTGCCTTTTGCTC		
TASK2	Forward	TCCTTACCAAGAGAGGTGTGA	202	NM_003740.3
	Reverse	TTCACACCGCCACAAAGT		
TASK3	Forward	TGTTCAAGCAGCTCTGCTCTC	122	XM_017013530.1
	Reverse	AGCGTGCCCATACATGGAA		
THIK1	Forward	CGTTTCCACCATAGGGTTTGG	86	NM_022054.3
	Reverse	AACACCAACAAGGCCGTAA		
THIK2	Forward	GTGGTGCAACCATAGGTTTCGG	109	NM_022055.1
	Reverse	TGAAGAACAGGATGGTCCAG		
TWIK1	Forward	GGGTGTGATCTCCGTAGTC	191	XM_011544184.2
	Reverse	ATATTGGGAGCCCCAGGCTT		
TWIK2	Forward	GAGCTGCACCCCTTCATTCT	125	XM_011527526.1
	Reverse	GAGCTGTCGTCCTGCGG		
TRAAK	Forward	AGATTAGCGTGGTGCCTGTC	193	NM_033310.2
	Reverse	GAGCTGTCGTCCTGCGG		
GAPDH	Forward	CTCCTGTTCGACAGTCAGC	89	NM_002046.5
	Reverse	GACTCCGACCTTCACCTTC		

NaH₂PO₄ and NaHCO₃ in experiments that used pH changes to test the sensitivity of the resting membrane potential (V_{rest}). The extracellular saline used to record inward rectifying K⁺ currents contained (in mM) 128 KCl, 1.5 MgCl₂, 1.5 CaCl₂, 1.25 NaH₂PO₄, 26 NaHCO₃, and 10 D-glucose. The intracellular (pipette) solution contained (in mM) 135 potassium D-gluconate, 10 KCl, 1 MgCl₂, 10 HEPES, 0.5 EGTA, 0.01 CaCl₂, 0.3 Na-GTP (pH 7.3, adjusted with KOH), and 1 Mg-ATP. All recordings were conducted at room temperature (22–24°C).

High-speed pressure clamp

Pressure pulses were generated with the high-speed system from ALA Scientific Instruments. Pressure steps were delivered through the patch pipette and controlled through pClamp 10.7. 100 μM 4,4'-Diisothiocyanatostibene-2,2'-disulfonic acid disodium salt (DIDS) was added to the extracellular solution to inhibit volume-regulated anion conductances.

Calcium imaging was conducted as described (Ryskamp et al., 2016; Jo et al., 2017; Phuong et al., 2017). Briefly, cells were loaded for 30–40 min with the calcium indicator Fura-2 acetoxyethyl ester (5 μM), placed in recording chambers on an upright epifluorescence microscope (Nikon E600 FN; 20×/0.5 or 40×/0.8 Nikon Fluor objectives), and perfused with isotonic saline containing (in mM) 126 NaCl, 2.5 KCl, 1.5 MgCl₂, 2 CaCl₂, 1.25 NaH₂PO₄, 26 NaHCO₃, and 10 D-glucose (300 mOsm; pH 7.4).

The high K⁺ external solution contained (in mM): 128 KCl, 1.5 MgCl₂, 1.5 CaCl₂, 1.25 NaH₂PO₄, 26 NaHCO₃, and 10 D-glucose. 340/380-nm excitation was delivered from a 150-W Xenon arc source (DG-4; Sutter Instruments). Fluorescence emission was high-pass filtered at 510 nm and captured with cooled EMCCD cameras (Photometrics). Data acquisition, ratio calculation, and background subtraction were accomplished using NIS Elements (Nikon). Results represent averages across cells (three to six slides, each containing 10–30 cells) from at least three separate experiments.

Measurement of hTM monolayer resistance

Real-time impedance of hTM monolayers was measured using the electric cell-substrate impedance sensing (ECIS) Z9 system (Applied BioPhysics), as described (Wang et al., 2016). In brief, cells were seeded on 8W10E+ arrays coated with rat collagen before seeding. Once a stable monolayer was established, the cells were exposed to test agents (TREK-1 activators and inhibitors) or control media, and the resistance was measured in each well for 1 h at 10-s intervals in response to a 4-kHz AC frequency (40 electrodes per well). Resistance for each well was normalized to the baseline resistance before the addition of agonist/antagonist to account for baseline differences in the electrodes. Treatment wells were normalized to the control resistance at each time point to determine change in resistance relative to control.

Statistics

The data are presented as mean \pm SEM. Student's *t* test and one-way ANOVA followed by Bonferroni post hoc test were used for analyses. Multiple comparisons were done by ANOVA. NS = $P > 0.05$; *, $P < 0.05$; **, $P < 0.01$; ***, $P < 0.001$; and ****, $P < 0.0001$.

Results

We investigated the intrinsic membrane properties, pressure sensitivity, calcium homeostasis, and monolayer impedance in juxtacanalicular hTM cells and validated a subset of the experiments in primary corneoscleral-derived cells prepared from nonglaucomatous human donors (pTM). The phenotype of primary and immortalized cells was validated with PCR analysis of TM-specific markers and steroid-induced up-regulation of myocilin (see Materials and methods).

Although the primate TM is a key regulator of IOP, its capacity for the regulation of fluid outflow is itself pressure sensitive (Brubaker, 1991; Acott et al., 2014), suggesting the potential presence of intrinsic mechanotransducers. To determine whether these include mechanosensitive ion channels, we evoked transmembrane currents with high-speed pressure clamp, a technique developed for the study of stretch- and pressure-activated channels (Sachs, 2010). The average V_{rest} recorded in the current clamp mode was -33.6 ± 1.2 mV for hTM ($n = 53$) and -29.4 ± 1.7 mV ($n = 16$) in pTM cells. The macroscopic current-voltage relationship showed low conductance at negative membrane potentials, conspicuous outward rectification, and reversal at -36.7 ± 2.4 mV (Fig. 1 A). Physiological pressure pulses (15 mm Hg; 3 s) evoked inward and outward currents at holding potentials of ± 100 mV (Fig. 1, A–D). Consistent with the recently proposed mechanosensing function of TRPV4 channels (Ryskamp et al., 2016), the amplitude of the pressure-evoked current was reduced by the selective antagonist HCO67047 (2 μ M; Fig. 1 E). The current-voltage relationship of the HCO67047-insensitive pressure-dependent current was dominated by an outwardly rectifying conductance (Fig. 1, F and G). Pressure steps induced a sustained negative shift of the reversal potential by approximately -15 mV, which was preceded by a transient depolarizing current (Fig. 1, H and I).

The implications of these findings are as follows. First, the observation that the TM resting potential (approximately -30 mV) is situated at the pressure-insensitive fulcrum for mechanosensitive channel activation predicts that the TM sensitivity to pressure is determined by the steady-state membrane potential. Second, TRPV4 channels partly mediate the pressure response. Third, pressure stimulation in the presence of TRPV4 inhibitors leaves a large residual outward conductance, indicating that TM mechanotransduction involves additional pressure-sensitive channels.

The TM resting potential is not maintained by canonical K⁺ channels

Given the key role of V_{rest} in TM pressure sensitivity (Fig. 1), we sought to determine the identity of ion channel subserving the resting membrane conductance. Under current clamp, patching cells with pipettes with K⁺ concentrations equimolar

to extrapipette saline abrogated the transmembrane potential gradient (Fig. 2 A). DIDS, an inhibitor of volume-regulated and voltage-operated anion channels, exerted a modest but statistically significant depolarizing shift (3.79 ± 0.63 mV; $n = 6$; not depicted), indicating that V_{rest} is principally a function of the K⁺ gradient. Mammalian TM cells express a variety of K⁺ channels (Lepple-Wienhues et al., 1991; Llobet et al., 2001; Gasull et al., 2003; Grant et al., 2013) but it is not clear which, if any, of these maintain or contribute to V_{rest} . Bath application of TEA (5 mM), a wide-spectrum blocker of voltage-gated (K_v), G protein-coupled inwardly rectifying and Ca²⁺-activated (K_{Ca}) K⁺ channels, reduced the outward current at nonphysiological ($+100$ mV) potentials from 494 ± 89 to 309 ± 44 pA (Fig. 2, B and C; $n = 6$ cells; $P < 0.05$); however, TEA had no effect on V_{rest} (Fig. 2 H). Similarly, 4-aminopyridine, a blocker of $K_v1.1$ (Shaker-related) K⁺ channels (1 mM), had no effect on V_{rest} (Fig. 2 H). To determine the role of Kir channels, we used hyperpolarizing ramps, which evoked inward currents ($n = 7/15$) that were suppressed by extracellular Cs⁺ (1 mM; $P < 0.05$; Fig. 2, D and E). The inwardly rectifying Cs⁺-sensitive current was also unmasked by high (145 mM) extracellular K⁺ (Fig. 2, F and G), yet extracellular supplementation of Cs⁺ had no discernable effects on V_{rest} (Fig. 2). These results demonstrate that K_v and K_{ir} channels in human TM cells can be activated at nonphysiological membrane potentials (± 100 mV, respectively) but do not contribute to V_{rest} . In addition, the low $[Ca^{2+}]_{TM}$ (~ 50 nM; Ryskamp et al., 2016) and TEA insensitivity argue against the potential involvement of K_{Ca} channels in V_{rest} maintenance.

The TM membrane potential is sensitive to a wide-spectrum blocker of K_{2P} channels

The K⁺ dependence of V_{rest} and insensitivity to classic K⁺ channel antagonists (Fig. 2 H) pointed at potential roles for the K_{2P} channel family, which has been associated with leak conductances in a variety of tissues, including smooth muscle cells, which share molecular markers with the TM (Enyedi and Czirjak, 2010; Stamer and Clark, 2017). The antimalarial alkaloid quinine (100 μ M), which is often used as a pan- K_{2P} channel blocker (Lesage and Lazdunski, 2000), depolarized hTM cells from -37.7 ± 4.4 to -8.7 ± 2.6 mV ($n = 7$; $P < 0.005$; Fig. 2, I and J) and evinced $\sim 57\%$ suppression of the outward current (Fig. 2, K–M). pTM V_{rest} and outward currents were similarly sensitive to quinine ($P < 0.01$ and $P < 0.001$ for V_{rest} and whole-cell currents, respectively; Fig. 2, J and M). These data indicate that the hyperpolarizing drive that maintains V_{rest} in human TM cells under physiological conditions is largely controlled by K_{2P} channels.

Molecular expression of KCNK channels in TM cells

The human K_{2P} channel family comprises at least 15 members that have been placed into six subfamilies based on sequence identity and functional characteristics. KCNK7 cannot be functionally expressed, TRESK is restricted to the spinal cord and brain, and TALK is confined to islets of Langerhans (Enyedi and Czirjak, 2010; Feliciangeli et al., 2015). Analysis of the remaining genes showed broadly consistent expression patterns across hTM/pTM cells, together with the expression of mRNA that encodes TRPV4,

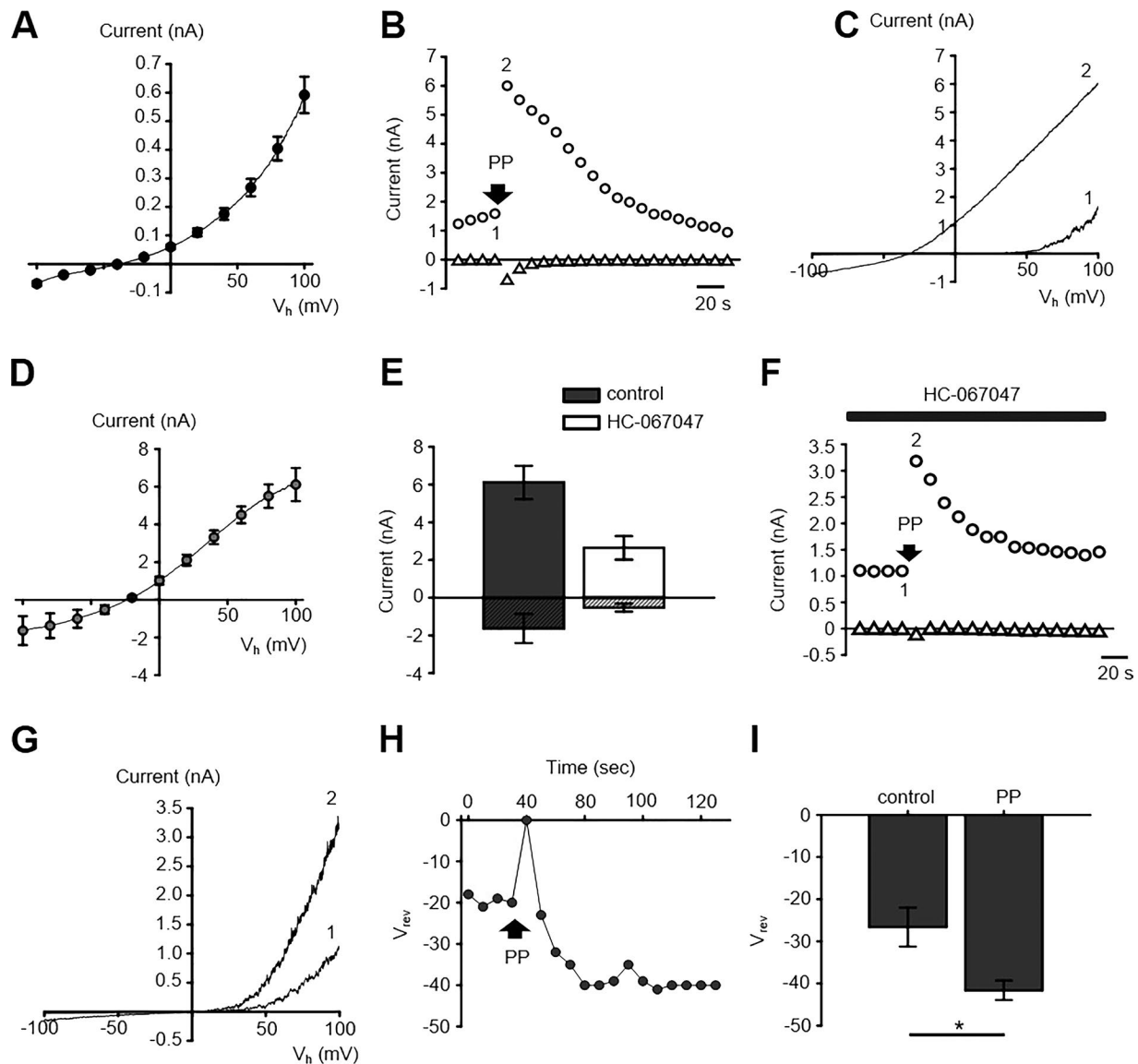


Figure 1. **Pressure-sensitive currents in TM cells involve a distinct type of mechanogated ion channels.** (A) I-V relationship of the whole-cell transmembrane conductance in TM cells; $n = 26$ cells. (B) Time course of pressure-sensitive currents. Pressure pulse (PP; 3-s duration) was applied at the time point indicated by an arrow. Shown are currents recorded at the holding potential (V_h) of -100 mV (triangles) and $+100$ mV (circles). (C) The I-V relationship of currents at time points indicated by the corresponding numbers in B. (D) Averaged I-V relationship of pressure-induced currents ($n = 5$) obtained by subtracting current recorded before PP from the peak response. (E) HC-067047 attenuates the pressure-induced current amplitude. Currents evoked at $V_h = 100$ mV and -100 mV are shown as open and patterned bars, respectively. (F) PP step (15 mm Hg; 3 s) in the presence of HC-067047 induces a small transient increase in the inward current and large outward current. Pressure application is denoted by arrow. (G) I-V relationship corresponding to the numeric markers in F. Pressure stimuli significantly increase the amplitude of outwardly rectifying current. (H) Representative time course of the pressure dependence of the membrane potential in the presence of HC-067047. PP transiently depolarizes the cell, an effect followed by sustained hyperpolarization. (I) Bar graphs summarizing results shown in H. Pair-sample t test, $n = 5$. Shown in A, D, E, and I are the mean \pm SEM values. *, $P < 0.05$.

a key TM mechanotransducer (Fig. 3 A). The most abundant K_{2P} transcripts belonged to TASK-1 (TWIK-related acid-sensitive K^+ channel; KCNK3), TREK-1 (TWIK-related K^+ channel, KCNK2), TWIK-2 (two-P domain in a weakly inward rectifying K^+ channel; KCNK6) and THIK-2 (tandem pore domain halothane-inhibited K^+ channel; KCNK12) subunits. Western blots confirmed TREK-1 protein expression (Fig. 3 C), with the expected bands (de la Peña et al., 2012) at 47 and 58 kD. Moreover, immunostaining showed that TREK-1 and TASK-1 localize to the TM plasma membrane (Fig. 3 D).

The TM membrane potential is dominated by arachidonate-sensitive channels

K_{2P} isoforms were functionally characterized using pharmacological tools. In particular, the long-chain polyunsaturated fatty acid AA is an activator of TREK-1, which also inhibits TASK-1 and TWIK-1 (Honoré et al., 2002; Heurteaux et al., 2004). Because AA also activates TRPV4 (Ryskamp et al., 2015) and modulates chloride channels (Meves, 2008), our experiments were generally conducted in the presence of HC-067047 (5 μ M), the pan-TRP blocker Ruthenium Red (RuR; 10 μ M), and/or DIDS

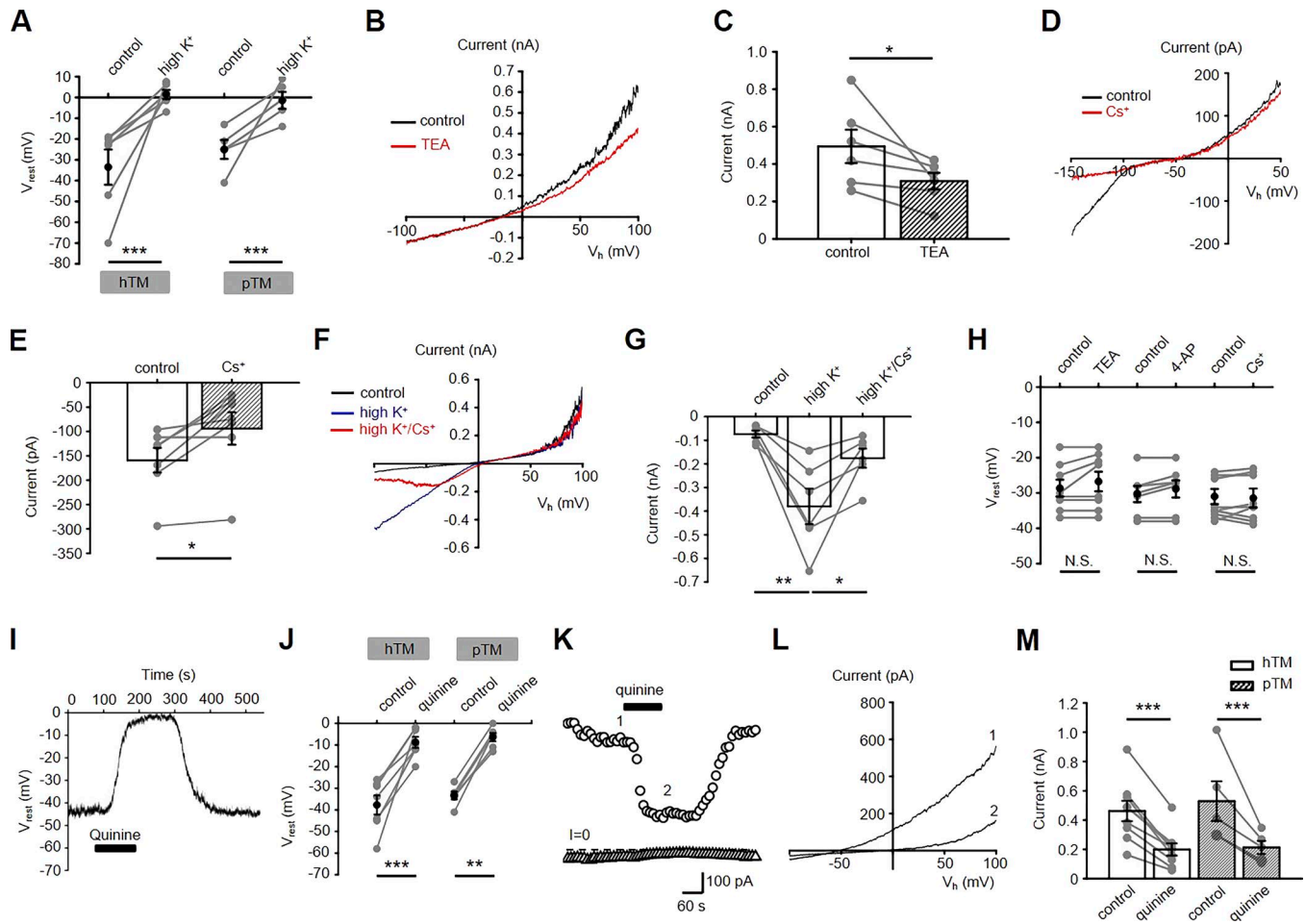


Figure 2. V_{rest} of TM cells is largely mediated by K_{2p} channels. (A) High K^+ depolarizes the membrane potential in hTM and pTM cells. Pair-sample t test, $n = 6$ cells for hTM and $n = 5$ for pTM. Gray symbols, individual values of V_{rest} ; black symbols, averaged data. (B) Representative traces showing the modest inhibitory effect of TEA (5 mM) on the outward current. (C) Averaged data for the effect of TEA on currents at $V_h = +100$ mV. Pair-sample t test, $n = 6$. (D) Cs^+ (1 mM) inhibits the hyperpolarization-activated whole-cell current. (E) Averaged data for the effect of Cs^+ on currents at $V_h = -100$ mV. Pair-sample t test, $n = 7$. (F) The inwardly rectifying K^+ conductance is facilitated by high K^+ , with the facilitated component sensitive to Cs^+ (1 mM). (G) Bar graphs summarizing the results shown in F. Pair-sample t test, $n = 6$ cells. (H) TEA (5 mM), 4-AP (1 mM), and Cs^+ (1 mM) have no effect on V_{rest} . The gray symbols indicate individual values of V_{rest} . Pair-sample t test, $n = 8$, $n = 8$, and $n = 7$ for TEA, 4-AP, and Cs^+ plots, respectively. (I) Representative trace demonstrating that V_{rest} is abrogated by quinine. (J) Quantification of quinine-evoked effects on V_{rest} in hTM and pTM cells. Gray symbols indicate individual V_{rest} values, black symbols show the means with \pm SEM. Pair-sample t test, $n = 8$ for hTM; $n = 9$ for pTM. (K) Representative time course of quinine-induced inhibition of the whole-cell current at $V_h = -100$ mV (triangles) and $+100$ mV (circles). (L) Current traces corresponding to the time courses marked in K. (M) Averaged hTM and pTM data for quinine-evoked inhibition of whole-cell currents at $V_h = +100$ mV. Pair-sample t test, $n = 9$ and $n = 5$ for hTM and pTM cells, respectively. Shown in A, C, E, G, H, J, and M are the mean \pm SEM values. N.S., $P > 0.05$; *, $P > 0.05$; **, $P > 0.01$; ***, $P > 0.001$.

to exclude the confounding contributions from cation/anion channels. Under these conditions, AA (100 μ M) evoked sustained hyperpolarizations (arrow in Fig. 4, A and B) that reduced V_{rest} from -24.2 ± 2.6 mV in unstimulated cells to -57.0 ± 4.6 mV ($n = 10$ cells; $P < 0.01$, paired t test). AA-evoked hyperpolarizations were associated with an increase in the outwardly rectifying conductance from 342.4 ± 49.0 pA in unstimulated cells to $2,078 \pm 213$ pA in the presence of the polyunsaturated fatty acid (Fig. 4, C and D). This effect was antagonized by spadin, a selective inhibitor of TREK-1 (Mazella et al., 2010), which reversibly depolarized the cells to -46.1 ± 4.8 mV ($n = 9$; Fig. 4, A and B) and partially but significantly ($P < 0.005$) suppressed the amplitude of AA-evoked outward currents (to $1,518 \pm 188$ pA; Fig. 4, C and D). The transient depolarization induced by AA in the presence of TRPV4 blockade (arrow in Fig. 4 A) was not

investigated further but could involve incomplete TRPV4 inhibition by micromolar HC-067047 and/or activation of arachidonate-regulated Ca^{2+} channels (e.g., Meves, 2008; Thompson and Shuttleworth, 2013).

We next explored whether the cohort of TREK-1 channels that maintain V_{rest} represents the maximal fraction of activatable channels by exposing the cells to small-molecule TREK-1 activators ML-335 and ML-402 (Lolicato et al., 2017). Both agonists shifted the membrane potential in the hyperpolarizing direction ($\Delta V_m = -15.5 \pm 4.1$ and -24.7 ± 6.5 mV by ML335 and ML-402, respectively) while augmenting the whole-cell conductance, with $\Delta I = 707 \pm 98$ and $1,458 \pm 159$ pA for ML-335 and ML-402, respectively (Fig. 5, A-E). Hence, TM cells maintain a substantial fraction of “reserve” TREK-1 channels that are available for activation.

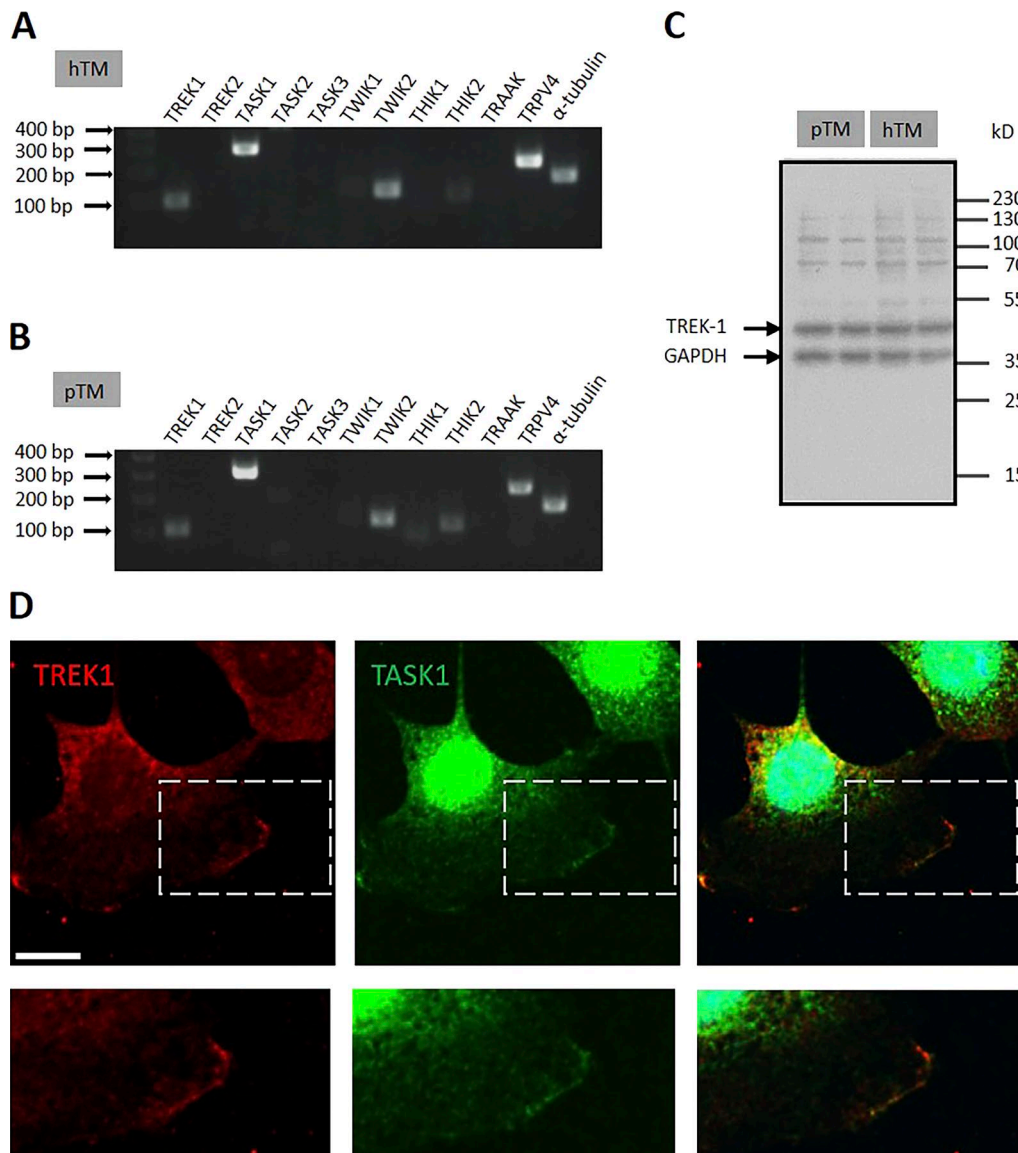


Figure 3. TM cells express K_{2p} transcripts and proteins. (A and B) Semiquantitative RT-PCR from hTM and pTM cells. K_{2p} mRNA expression patterns reveal the presence of TREK-1, TASK-1, TWIK-2, and THIK-2 mRNAs, and strong expression of TRPV4 together with the reference α -tubulin mRNA (representative of two to three experiments). (C) Western blots from hTM and pTM samples show the expression of TREK-1 protein. (D) Immunocytochemistry; hTM cells double-labeled for TREK-1 and TASK-1. Upper panel: TREK-1 (Alexa Fluor 594 nm) and TASK-1 (Alexa Fluor 488 nm) are localized to the plasma membrane. Lower panel: Magnified images of the regions shown in the upper panel.

TREK isoforms have been differentiated from other K_{2p} channels with the dihydropyridine analogue amlodipine (Liu et al., 2007). The blocker (10 μ M) depolarized hTM cells from -33.4 ± 3.9 to -4.1 ± 1.7 mV and attenuated the amplitude of the outward current (Fig. 5, F–J). Similar inhibitory effects on the membrane potential and outward conductance were observed in pTM cells (Fig. 5, G and I), confirming that V_{rest} is largely subserved by tonic activation of TREK-1.

The prominent mRNA and protein expression of TREK-1 and TASK-1 in pTM/hTM cells (Fig. 3) prompted us to clarify their relative contributions to V_{rest} with isoform-specific knockdown. Cells were transfected with lentiviral vectors carrying shRNA or scrambled (Sc) RNAs that were labeled with a fluorescent marker (GFP). Transcript analysis showed 0.57 ± 0.2 knockdown

of TREK-1 ($P < 0.2$) and 0.43 ± 0.02 TASK-1 mRNAs ($P < 0.0018$) relative to Sc controls, with no apparent effects on cell morphology or survival. Cells transfected with Sc shRNA expressed the outwardly rectifying current (Fig. 6, B and C) typical of untransfected hTM/pTM (Fig. 1 A). Transfection with Sc shRNA had no effect on V_{rest} (-29.1 ± 2.9 mV), whereas TREK-1 knockdown depolarized the cells to -16.9 ± 2.1 mV (Fig. 6 A). TASK-1 knockdown had no significant effect on V_{rest} (Fig. 6 D). The transmembrane current in TREK-1 shRNA-transfected cells at $V_h = 100$ mV was reduced from 480 ± 60 pA in cells overexpressing Sc shRNA to 187 ± 23 pA in TREK-1 shRNA-expressing cells (Fig. 6, A and B). Down-regulation of TASK-1 had a slight but significant depolarizing effect on V_{rest} in pTM cells ($P < 0.05$; Fig. 6 J). Similar results were obtained from pTM cells (Fig. 6, G–L). These data confirm

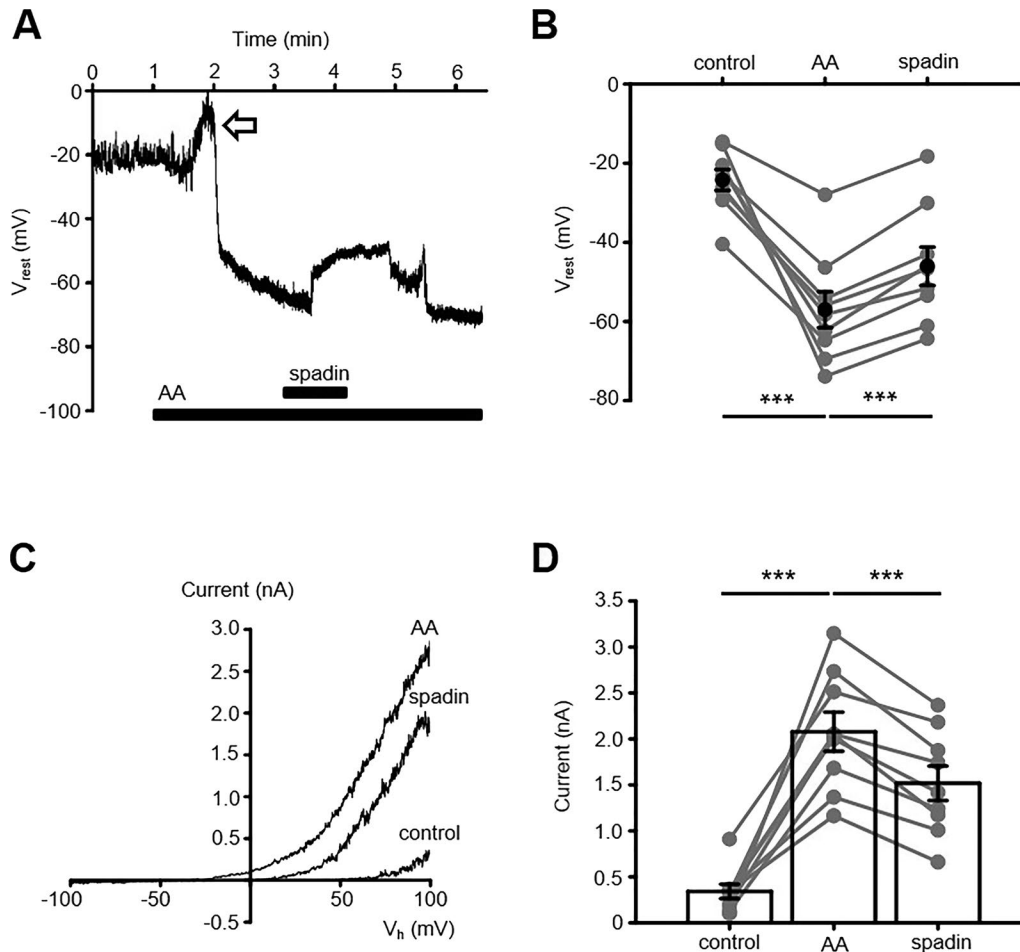


Figure 4. **TM membrane potential is potently modulated by arachidonate-activated currents.** (A) Current clamp, hTM cells superfused with the TRPV4 blocker HC-067047 (2 μ M). AA transiently depolarizes the cell, an effect followed by sustained hyperpolarization that is partially and reversibly antagonized by spadin (1 μ M). (B) Quantification of experiments shown in A at 3 min after AA application. The black symbols show the mean \pm SEM. Pair-sample *t* test, *n* = 9 cells. (C) The I-V relationship of the AA-evoked current shows an increase in the outward conductance that is sensitive to spadin. (D) Data summary for the experiments shown in C. The black symbols show the mean \pm SEM values of currents recorded at +100 mV. Pair-sample *t* test, *n* = 9 cells. ***, *P* < 0.001 in C and D.

the dominant contribution of TREK-1 to the background “leak” conductance in TM cells and suggest a potential auxiliary role for TASK-1 in primary cells.

TREK-1 channels are required for TM pressure sensitivity

We investigated the role of K_{2P} channels in mediating the TM responsiveness to physiological steps of pressure in the presence of HC-067047. Positive pressure steps (15 mm Hg, 3 s) hyperpolarized the V_{rest} by 3.52 ± 1.49 mV (*n* = 8 cells, *P* < 0.05; Fig. 7, A and B), evoking robust outward currents that reached the peak of $2,645 \pm 624$ pA within 10 s (*n* = 5; Fig. 7 C). Consistent with K_{2P} involvement, quinine reduced the pressure-evoked outward current by \sim 86% to 369 ± 78 pA (*n* = 5 and *n* = 6 cells for control and quinine groups, respectively; *P* < 0.01; Fig. 7, C and D). Given that TREK-1 is the sole TM-expressed member of the mechanosensitive K_{2P} group activated by poking, stretching, or pressuring the plasma membrane (Dyachenko et al., 2006; Brohawn et al., 2014), we assessed the pressure response after its knockdown. The pressure-induced current in control Sc-shRNA-transfected cells ($3,412 \pm 552$ pA) was attenuated by \sim 80% to 686 ± 63 pA after the transfection with TREK-1 shRNA (*n* = 11 for Sc shRNA and *n*

= 11 for TREK-1 shRNA groups; respectively, *P* < 0.01; Fig. 7, E and F). Collectively, these results identify TREK-1 as a regulator of TM mechanosensitivity.

Inhibition of K_{2P} channels results in an elevation of intracellular Ca^{2+}

Given the dominant role of the second messenger calcium in TM transmembrane ion flux, volume regulation, contractility, and outflow resistance (Wiederholt et al., 2000; Gasull et al., 2003; Dismuke and Ellis, 2009; Ryskamp et al., 2016), we wondered whether TREK-1 activation coincides with altered Ca^{2+} homeostasis. To test this, cells were loaded with the calcium indicator Fura-2 AM, and the 340/380-nm fluorescence ratio was monitored in the presence of TREK-1 activators and blockers.

Unexpectedly, exposure to the TREK-1 activator ML-402 (40 μ M) evoked rapid $[Ca^{2+}]_i$ elevations in \sim 85% of hTM cells (Fig. 8, A and B). This effect was abolished by RuR (10 μ M), suggesting that TREK-1-dependent hyperpolarizations stimulate Ca^{2+} entry via tonically activated TRP-like channels (Fig. 8 C). We tested this possibility in voltage-clamped cells by switching the membrane potential from -30 to 0 mV and -70 mV, respectively.

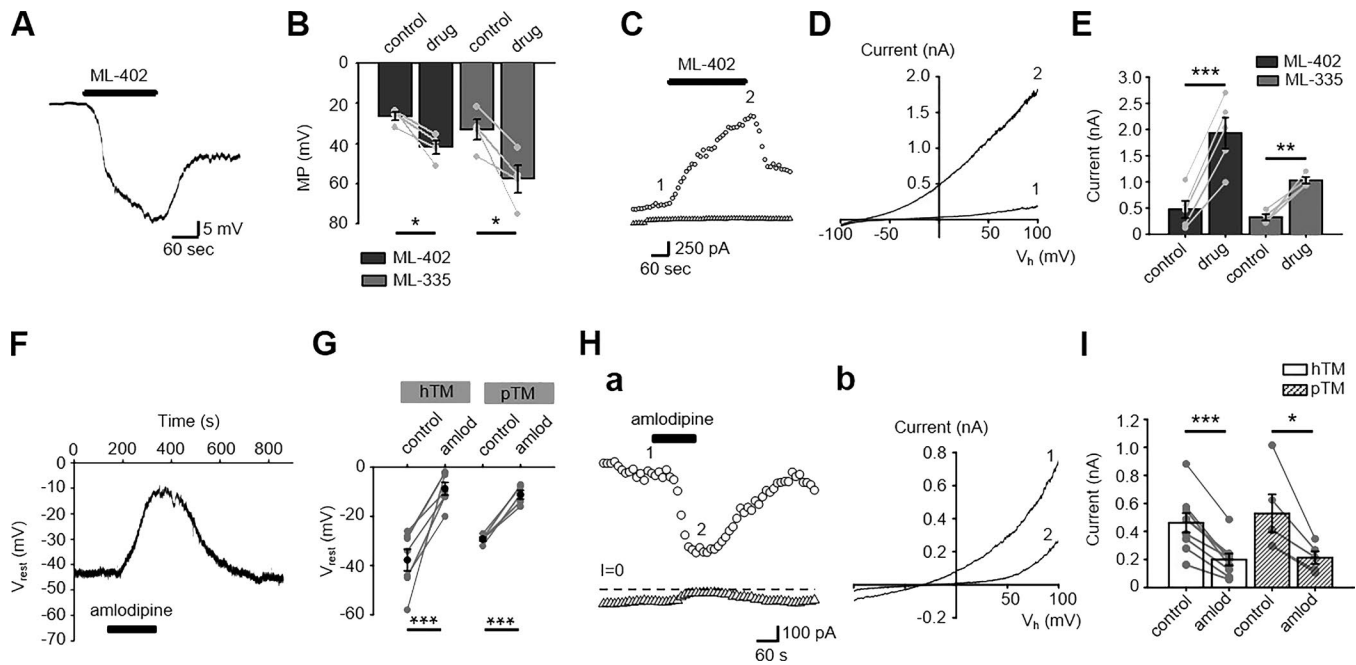


Figure 5. V_{rest} and transmembrane conductance are a function of TREK-1 activation. (A) Current clamp, hTM cells. The selective TREK-1 agonist ML-402 evoked a rapid and large hyperpolarization. (B) Quantification of the effects of ML-402 and ML-335 on the membrane potential. Pair-sample *t* test. *n* = 4 and *n* = 4 for ML-402 and ML-335, respectively. (C) Voltage clamp. Representative time course of the whole-cell current evoked by the TREK-1 agonist ML-402 (40 μ M) at V_h = -100 mV (triangles) and +100 mV (circles). (D) I-V relationship for the currents recorded in C shows dramatic potentiation of the outward conductance. (E) Averaged data for the ML-402 and ML-335 effect on the whole-cell current. Pair-sample *t* test; *n* = 5 cells and *n* = 4 cells for ML-402 and ML-335, respectively. (F) Current clamp. The TREK-1 blocker amlodipine depolarizes the hTM membrane potential. (G) Data summary for the amlodipine effect in hTM and pTM cells. Pair-sample *t* test; *n* = 7 and *n* = 5 for hTM and pTM, respectively. (H) Voltage clamp, hTM. The time course and the I-V relationship of amlodipine modulation of the whole-cell current. Current amplitudes at V_h = -100 mV (triangles) and +100 mV (circles; a); traces corresponding to indicated time points (b). (I) Data summary for amlodipine-induced suppression of the steady-state TM current. Shown are mean \pm SEM values for the holding potential of +100 mV paired *t* test. *n* = 9 cells and *n* = 5 cells for hTM and pTM, respectively. Shown in B, E, G, and I are the mean \pm SEM values. *, *P* < 0.05, ***, *P* < 0.001.

Consistent with the hypothesis that the cells experience constitutive TRP-mediated Ca^{2+} influx driven by the electrochemical gradient, we found that depolarizing steps decreased $[Ca^{2+}]_i$, whereas hyperpolarizations, conversely, increased $[Ca^{2+}]_i$. Reductions ($-\Delta 1.8$ mM) and increases ($+\Delta 3$ mM) in $[Ca^{2+}]_o$ induced corresponding decreases and increases in $[Ca^{2+}]_i$ (Fig. 8 D). Another surprising observation was that TREK-1 inhibitors quinine, amlodipine, and spadin also evoke robust increases in $[Ca^{2+}]_i$ in resting TM cells (Fig. 8, G-H). The source of Ca^{2+} signals induced by TREK-1 blockers remains to be determined but may include depolarization-activated Ca^{2+} channels and/or release from internal stores (e.g., Wiederholt et al., 2000).

TREK-1 regulates impedance of TM monolayers

To determine whether channel activators and inhibitors have an impact on the transcellular current flow in TM monolayers, we used ECIS. We have recently used this technique in endothelial monolayers to characterize the permeability of adherens junctions (Phuong et al., 2017), but current flow across nonendothelial monolayers that lack intercellular junctions was proposed to largely represent contractility-dependent adhesivity to the substrate (Qiu et al., 2008; Ramachandran et al., 2011). As illustrated in Fig. 9, 30-min exposure to TREK-1 agonists ML402 and ML67-33 that had been pipetted into the well dose-dependently lowered monolayer impedance. At 100 μ M, ML402 and ML67-33 reduced normalized impedance by $9.0 \pm 1.7\%$ and $19.0 \pm 2.6\%$ (*n* =

4), respectively (Fig. 9, A-D). The effect of ML402 was transient, whereas ML67-33 demonstrated more sustained reduction of impedance without apparent recovery in the presence of the drug.

Similar to its effect on Ca^{2+} signals, K_{2P} inhibition likewise decreased the impedance of TM monolayers, with $0.6 \pm 0.2\%$ (*n* = 7) and $10.0 \pm 1.4\%$ decreases in peak impedance (*n* = 8) observed at 10 and 100 μ M quinine (Fig. 9, E and F). In contrast to the effect of ML67-33, the effect of quinine was time dependent, as translayer impedance largely recovered in the presence of the drug. The observed TREK-1-dependent reductions in cell-substrate impedance are consistent with increased paracellular spacing between adjacent TM cells, altered cell contractility, and/or changes in cell-matrix adhesion and support a role for TREK-1 in TM-ECM interactions (Goel et al., 2012).

Discussion

We report that polymodal TREK-1 channels are required to maintain the membrane potential, Ca^{2+} homeostasis, and pressure sensitivity in human TM cells. Our findings include (a) the close relationship between the TM membrane potential and pressure sensitivity; (b) TREK-1 activation underlies the steady-state resting potential, with a reserve pool of nonactivated channels mediating the hyperpolarizing response to pressure and PUFAs; (c) novel links between TREK-1 activation and Ca^{2+} homeostasis; and (d) TREK-1 regulates cell-ECM adhesivity. Together, these results

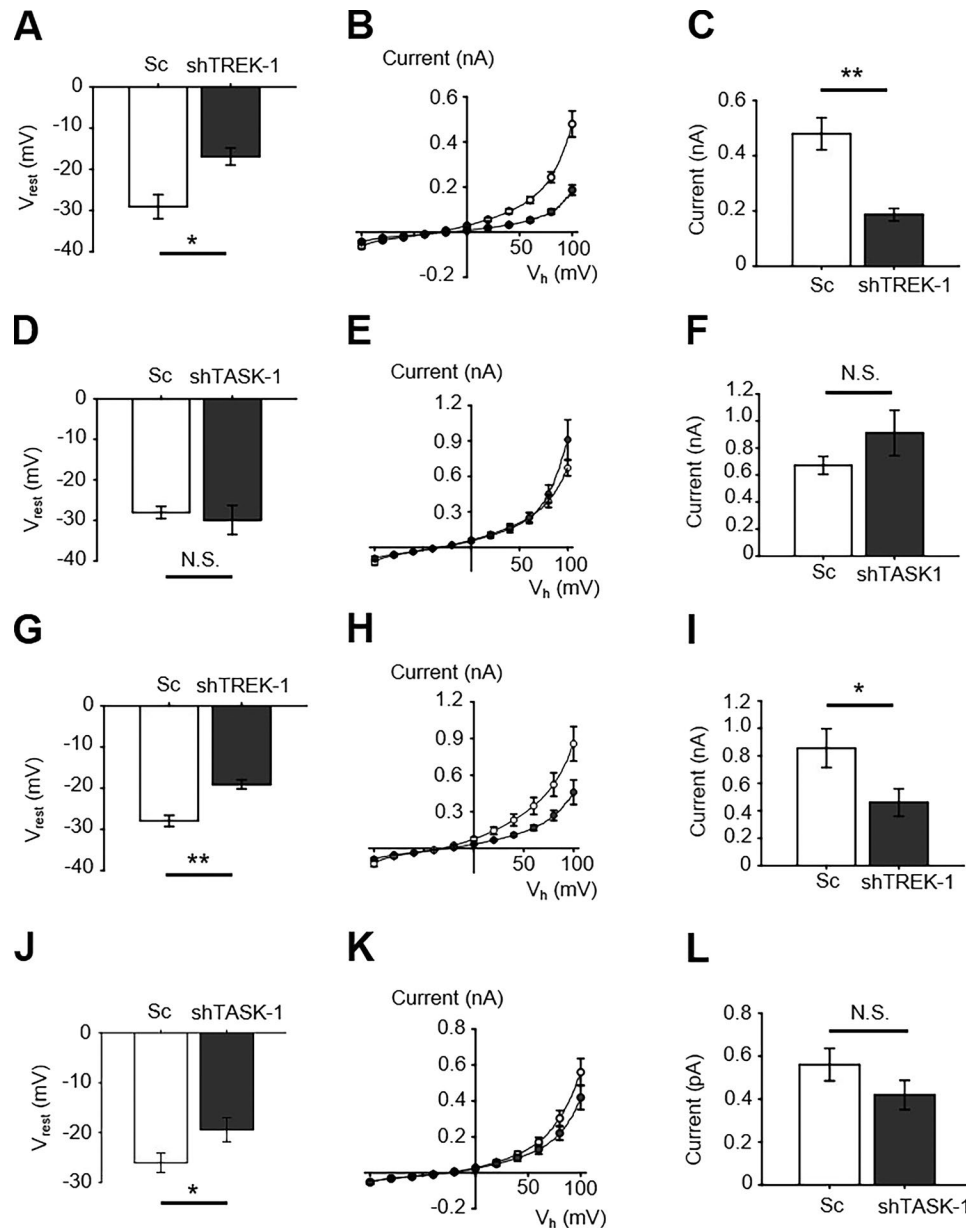


Figure 6. TREK-1 but not TASK-1 knockdown suppresses the transmembrane conductance and depolarizes V_{rest} in hTM cells. (A) Current clamp, hTM cells. Averaged V_{rest} values in cells transfected with scrambled (Sc) shRNA ($n = 12$ cells) or TREK-1 shRNA (shTREK-1; $n = 10$ cells); two-sample t test. (B) Voltage clamp. Averaged I-V relationship for cells transfected with Sc ($n = 12$ cells; open circles) or shTREK-1 ($n = 10$ cells; closed circles). (C) Quantification of the TREK-1 dependence of the steady-state current. The current amplitude was significantly reduced by TREK-1 knockdown ($n = 12$ cells and $n = 10$ cells for Sc- and shTREK-1 cohorts, respectively). (D) Current clamp. Averaged V_{rest} values in cells transfected with scrambled (Sc) shRNA (Sc; $n = 10$) or TASK-1 shRNA (shTASK-1; $n = 10$), shown as mean \pm SEM. $P > 0.05$, two-sample t test. (E) Voltage clamp. Averaged I-V relationship for cells transfected with Sc ($n = 10$) or shTASK-1 ($n = 10$). (F) Quantification of TASK-1 dependence of the steady-state current in hTM cells. The whole-cell current amplitude was unaffected by TASK-1 knockdown. $P > 0.05$, two-sample t test. (G) Current clamp, pTM. Averaged V_{rest} for Sc-shRNA ($n = 11$) and TREK-1 shRNA (shTREK-1; $n = 11$) transfected pTM cells, with mean \pm SEM. *, $P < 0.05$, two-sample t test. (H) Voltage clamp. Averaged I-V curve for Sc ($n = 11$) and shTREK-1 ($n = 11$) transfected cells. (I) Quantification of TREK-1 dependence of the steady-state current in pTM cells ($n = 11$ and 11 cells for Sc and shTREK-1 cohorts, respectively). *, $P < 0.05$, two-sample t test. (J) Current clamp, pTM. Averaged I-V curve for Sc ($n = 20$ cells) and TASK-1 shRNA ($n = 22$ cells) transfected cells. Two-sample t test. (K) Voltage clamp. Averaged I-V curve for Sc ($n = 20$ cells) and shTASK-1 ($n = 22$ cells) transfected pTM cells. (L) Quantification of TASK-1 dependence of the steady-state current in pTM cells. $n = 20$ cells and $n = 22$ cells for scrambled control and shTASK-1 cohorts, respectively. Two-sample t test. Shown in A–L are the mean \pm SEM. N.S., $P > 0.05$; *, $P < 0.05$; **, $P < 0.01$.

place TREK-1 in the center of mechanosensing and IOP regulation in the primate eye.

The current-voltage relationship and outward rectification of the macroscopic leak current in physiological K^+ gradients, together with the abrogation of the membrane potential gradi-

ent in symmetric transmembrane K^+ gradients, indicate that TM V_{rest} is controlled by the passive behavior of K^+ leak channels predicted by the Goldman–Hodgkin–Katz equation. Among the variety of K^+ channels expressed in bovine, mouse, and/or human TM cells are voltage-activated, inwardly rectifying, ATP-sensi-

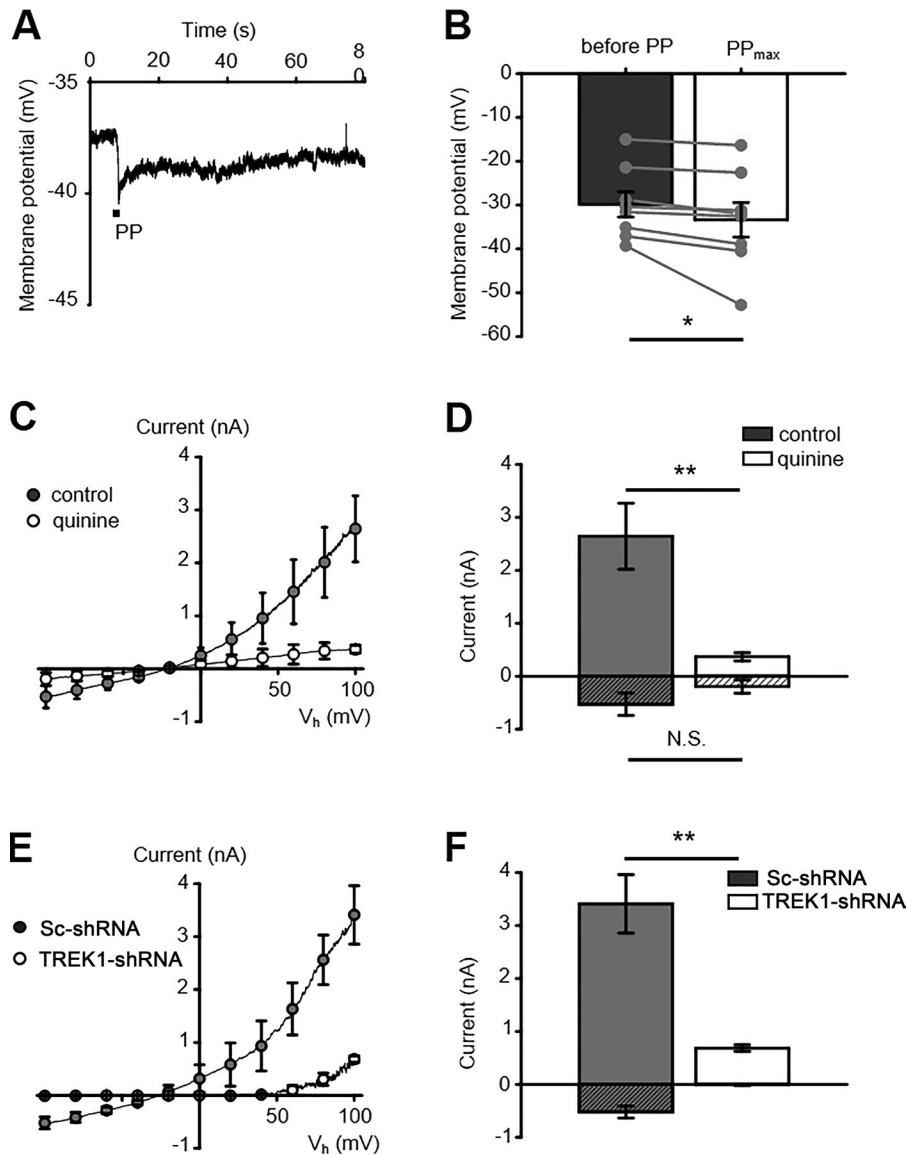


Figure 7. TREK-1 is a principal TM mechano-transducer. (A) Representative current-clamp recording in the presence of HC067047. Pressure pulse (PP, 2 s, 15 mm Hg) hyperpolarizes the membrane potential. (B) Quantification of experiments from A. $n = 8$ pair-sample t test. (C) Voltage clamp, pTM. The I-V relationship for pressure-induced currents in control (gray circles) and quinine-treated (white circles) cells shows that the pan- K_{2P} blocker induces a significant reduction in the amplitude of the pressure-evoked current. (D) Averaged amplitude of pressure-induced currents at $V_h = -100$ mV (patterned bars) and 100 mV (open bars) for control and quinine-treated cells. Two-sample t test, $n = 5$ cells and $n = 6$ cells for control and quinine-treated cohorts, respectively. (E) pTM. TREK-1 but not Sc shRNA reduces the amplitude of pressure-induced currents. (F) Quantification of pressure-evoked currents at $V_h = -100$ mV (patterned bars) and +100 mV (open bars) in cells transfected with Sc and TREK-1 shRNA. Two-sample t test, $n = 11$ cells and $n = 11$ cells for Sc and TREK-1 shRNA cohorts, respectively. Shown in B–D are the mean \pm SEM values. N.S., $P > 0.05$; *, $P < 0.05$; **, $P < 0.01$.

tive, Ca^{2+} -activated large-conductance (BK) and tandem pore K^+ channels (Llobet et al., 2001; Gasull et al., 2003; Grant et al., 2013), and volume-activated K^+ channels (Mitchell et al., 2002). Our observation that resting K^+ fluxes in hTM/pTM cells are insensitive to classic blockers of K_v , K_{ir} , and K_{Ca} channels supports the conclusion that the hyperpolarizing component of the V_{rest} is subserved almost exclusively by K_{2P} channels. We identified TREK-1 as the key regulator of the background conductance based on the following evidence: (a) hyperpolarizations induced by AA, pressure, and small-molecule activators; (b) obliteration of the resting potential by amlodipine, spadin, and TREK-1:shRNA; (c) outward rectification of the TM current typical of TREK-1 activation in the presence of divalent cations (Maingret et al., 2002); and (d) antibody staining in cultured cells (Fig. 3) and intact tissue (Carreon et al., 2017). We were unable to discern obvious roles for TWIK/THIK-2 subunits, which may have been nonfunctional under our experimental conditions (Bichet et al., 2015), whereas TASK-1 may contribute a small residual outward component in pTM cells.

The extent to which TREK-1 dominates the TM membrane potential seems to be without precedent in eukaryotic cells. Typically, the channel is expressed in cells from organs that experience mechanical deformation (e.g., lung, uterus, stomach, intestine, colon, retinal, and bladder cells), but its contribution to V_{rest} tends to be auxiliary (Fink et al., 1996; Reyes et al., 1998; Ferroni et al., 2003; Heurteaux et al., 2004; Honoré, 2007; Lembrechts et al., 2011; Cadaveira-Mosquera et al., 2012; Lei et al., 2014). Submaximal TREK-1 activation in resting TM cells may be caused by the low probability of opening at near-zero membrane tension (Fink et al., 1996), whereas TREK-1-mediated hyperpolarizations (~15–25 mV) induced by pressure, AA, and selective agonists indicate a substantial pool of activatable channels. Activation of this reserve pool might endow the TM with autoregulatory response to mechanical stressors, as documented in heterologously expressing cells (Brohawn et al., 2014). Chloride channels almost certainly contribute to the maintenance of the hyperpolarized state, because blocking Cl^- -permeable channels (e.g., volume-regulated anion channels, $ClC2$ and $ClC3$; Mitchell

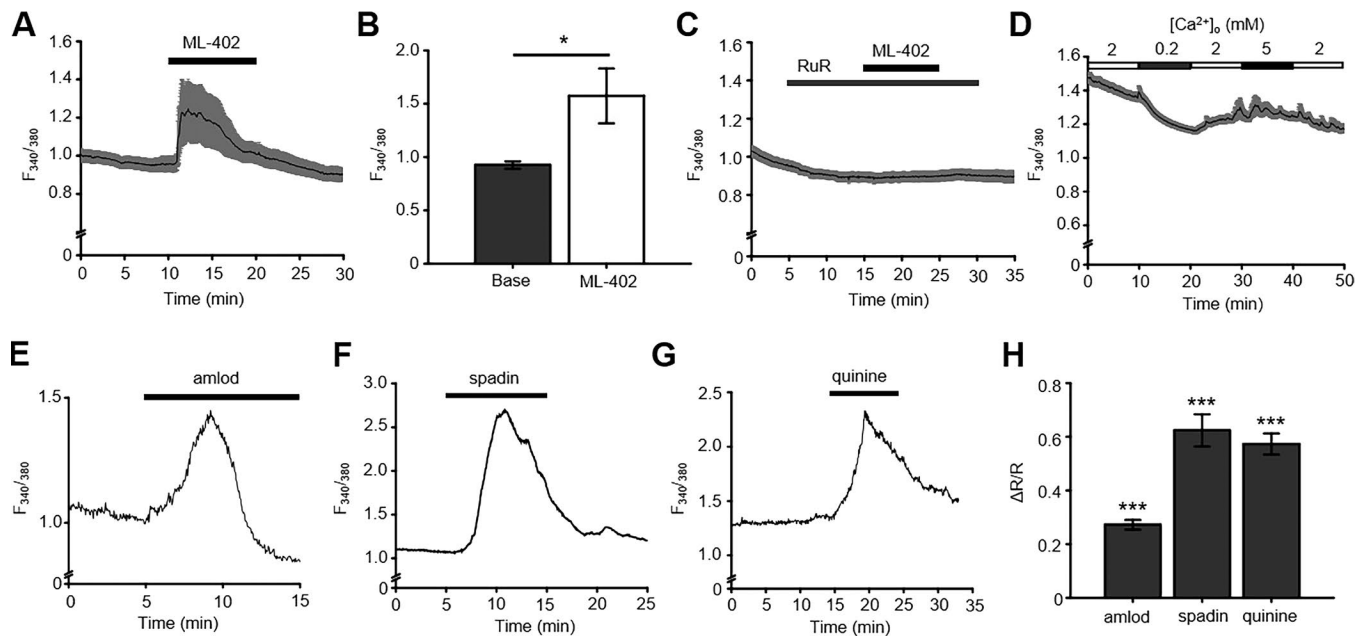


Figure 8. **TREK-1 activation and inhibition is coupled to TM Ca^{2+} homeostasis.** (A) Fura-2 AM loaded hTM cells. The TREK activator ML-402 (40 μ M) evokes sustained elevation in $[Ca^{2+}]_i$ ($n = 27$ cells; pooled responses from 23 responders and 4 nonresponders in the field of view). (B) Bar graphs summarizing the experiments in A. Pair-sample t test. (C) ML-402-evoked $[Ca^{2+}]_i$ elevations are abolished by RuR (10 μ M; $n = 28$ cells). (D) $[Ca^{2+}]_i$ is a function of the driving force for Ca^{2+} influx. $F_{340/380}$ ratios are plotted as extracellular Ca^{2+} concentrations. $[Ca^{2+}]_o$ were altered between 0.2 and 5 mM. (E–G) Representative $F_{340/380}$ traces illustrating effects of TREK-1 inhibitors amlodipine, spadin, and quinine, respectively, on $[Ca^{2+}]_i$. (H) Summary of the data shown in E–G. $n > 60$ cells for each group. Shown in A–D and H are the mean \pm SEM values. *, $P < 0.05$; ***, $P < 0.001$.

et al., 2002; Comes et al., 2005) evinced small (~ 4 –6 mV) depolarizations (O. Yarishkin and D. Križaj, unpublished observations). Studies in bovine TM cells similarly suggested that Cl^- fluxes supply $\sim 10\%$ of the standing outward current (Wiederholt et al., 2000). Another interesting question pertains to the nature of the depolarizing component that balances the resting K^+ and Cl^- fluxes. The identity of this component remains to be determined, with candidates including voltage-operated, store-operated Orai and/or TRP channels (Wiederholt et al., 2000; Abad et al., 2008; Tran et al., 2014).

In addition to maintaining V_{rest} , the TREK-1 response to pressure appears to modulate calcium influx and cell–ECM interactions. ECIS measurements revealed that channel agonists and antagonists induced significant decreases in monolayer impedance, with a time course that roughly matched that of the $[Ca^{2+}]_i$ elevations evoked by TREK-1 activation and inhibition. The precise mechanism remains to be determined but may have involved Ca^{2+} -dependent changes in TM contractility, integrin binding (Wiederholt et al., 2000; Campbell and Humphries, 2011), and/or integrin–ECM contacts (Ramachandran et al., 2011), given that Ca^{2+} regulates the interactions between TREK-1 and α -smooth muscle cell actin (Patel et al., 1998), MAPK activation (Bittner et al., 2013), strain-dependent formation of actin stress fibers, and secretion of fibronectin (Ryskamp et al., 2016). Low levels of VE cadherin and lack of adherens and occludens contacts (Bhatt et al., 1995; Pattabiraman et al., 2014) might have contributed to the low steady-state impedance compared with endothelial monolayers (Phuong et al., 2017) that is further decreased through TREK-1 modulation. It remains to be seen whether the increased impedance observed in glaucoma-

tous cells (Torrejon et al., 2016) is mirrored by altered TREK-1 activation in hypertensive eyes.

Among the advantages of the high-speed pressure clamp technique over traditional cell poking assays is the ability to precisely control the timing and amount of force applied to the channel. Using this method, we found hyperpolarizations evoked by physiological pressure steps to be driven mainly by TREK-1. Because the unpressurized gigaseal patch itself imposes nonzero lateral tension on the channel, we did not estimate the threshold for activation by pressure. It is notable that forces that activate TREK-1 (Brohawn et al., 2014) also span the IOPs measured in the healthy eye, ranging from ~ 3 –7-mm diurnal fluctuations to transient ~ 200 –300-mm Hg increases evoked by blinking, saccadic eye movements, eye scratching, and sneezing (Downs, 2015). The pressure steps used in our study (15 mm Hg) increased the open probability of human TREK-1 by ~ 19 -fold (Lei et al., 2014), but it remains to be determined how its open probability is influenced by membrane tensions in hypertensive eyes in which TM cells are stiffer (Last et al., 2011; Pattabiraman et al., 2014) and whether gain/loss-of-function TREK-1 mutations contribute to hypertensive injury in the eye (e.g., Goel et al., 2012; Decher et al., 2017).

One of the conclusions of the present study is that TREK-1 in healthy TM cells functions as a voltage tuner that minimizes pressure responsiveness, Ca^{2+} dysregulation, and contractility through its control of V_{rest} (approximately -30 mV in human and bovine TM cells; Lepple-Wienhues et al., 1994; Llobet et al., 2001). Tensile steady-state may be so important for TM cells that deviations in depolarizing or hyperpolarizing directions induce a similar compensatory (calcium) response; however, we demonstrate that these compensatory responses involve

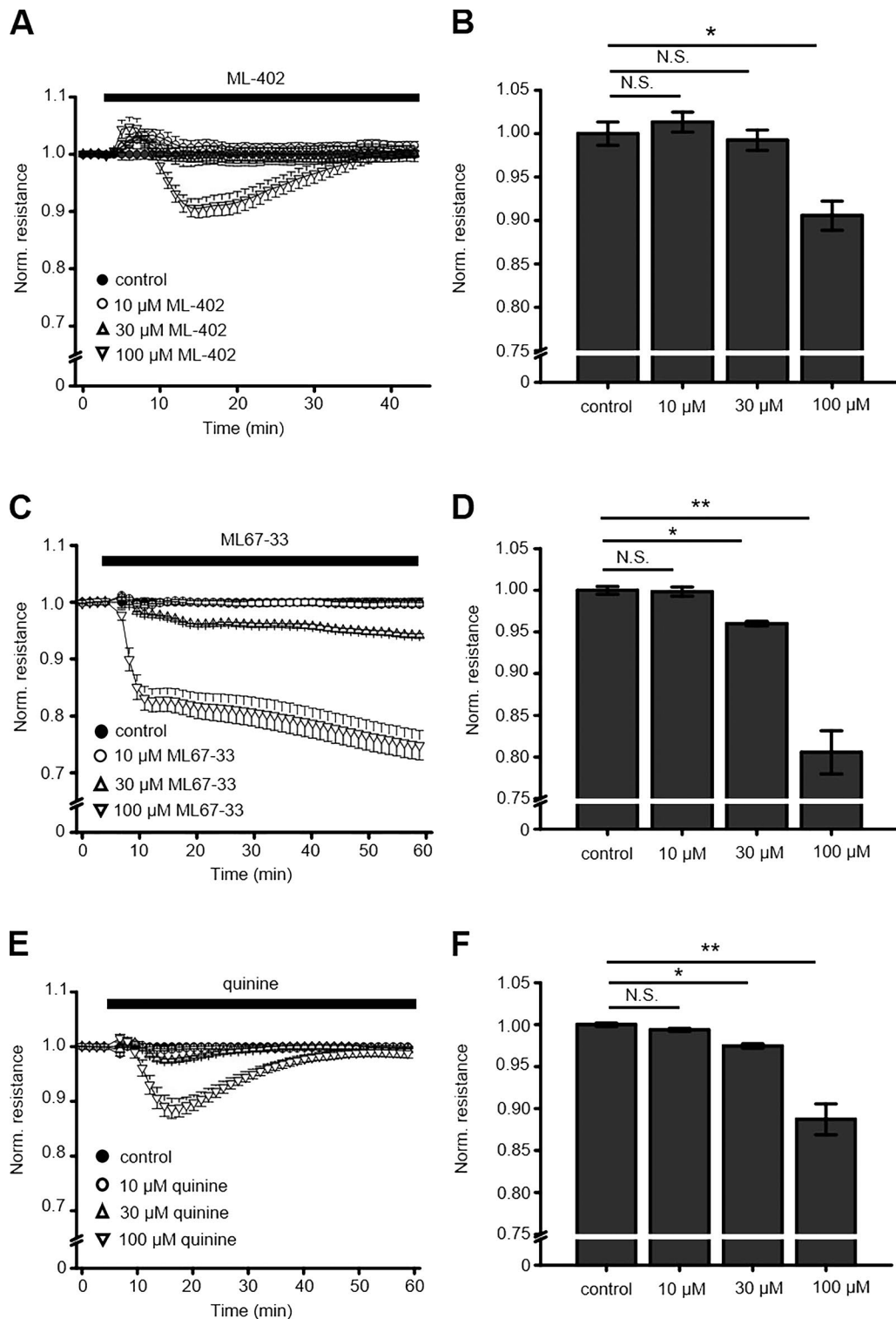


Figure 9. **TREK-1 modulates cell-ECM interactions.** (A and C) Time courses of hTM monolayer impedance in the presence of TREK-1 agonists ML-402 and ML67-33. TREK-1 activation dose-dependently decreases monolayer impedance. (B and D) Quantification of results shown in A and C ($n = 2-3$). (E) Quinine dose-dependently lowers the TM monolayer impedance. (F) Summary of results shown in E. Two-sample t test. Shown in A-F are the mean \pm SEM values. N.S., $P > 0.05$; *, $P < 0.05$; **, $P < 0.01$.

different intracellular signaling pathways. RuR sensitivity of the hyperpolarizing response suggests that TREK-1 activators facilitate TRP channel-dependent Ca^{2+} influx, possibly via TRPV and/or TRPC channels (Abad et al., 2008; Ryskamp et al.,

2016), whereas TREK-1 inhibition presumably depolarizes the cells and induces voltage-dependent Ca^{2+} influx (e.g., Lepple-Wienhues et al., 1991). This ingenious molecular arrangement allows TREK-1 to transduce decreases and increases in pres-

sure into calcium-dependent compensation to modulate TM tensile homeostasis.

We hypothesize that IOP-dependent tensional integration of the TM membrane involves concurrent modulation of at least two intrinsic mechanotransducers, TREK-1 and TRPV4. Compressive, tensile, and/or shear loading prestress the TM membrane by influencing its curvature and fluidity (Anishkin et al., 2014) and thereby facilitating force detection at the TREK-1–lipid interface. In contrast to TREK-1, TRPV4 channels do not regulate the standing conductance, calcium homeostasis, or pressure sensing, as indicated by the lack of effect of HCO67047 on the V_{rest} $[Ca^{2+}]_i$, and resting IOP (Ryskamp et al., 2016). After the decrease in outflow facility, changes in aqueous shear flow, and/or changes in membrane stiffness that elevate IOP, both TRPV4 (Lakk et al., 2017) and TREK-1 (Brohawn et al., 2014) are activated and cooperate to set a new homeostatic tensile set point. We propose that such set points are likely to be modulated by phospholipid hydrolysis via phospholipase A2 and production of AA (C20:4 ω 6), which regulates both TRPV4 and TREK-1. It is noteworthy that exposure to AA recapitulates many aspects of TRPV4- and TREK-1-induced cytoskeletal remodeling, including increases in $[Ca^{2+}]_i$, up-regulation of actin stress fibers, and fibronectin release (Ryskamp et al., 2016; White et al., 2016; Carreon et al., 2017), whereas inhibition of AA production weakens stress fibers and increases aqueous fluid outflow (Pattabiraman et al., 2014). Hence, IOP elevations might regulate the channels directly through force transmission or indirectly through AA and its eicosanoid metabolites (Weinreb et al., 1988; Kirber et al., 1992; Maingret et al., 1999; Enyedi and Czirják, 2010; Ryskamp et al., 2014; Jo et al., 2016). Interestingly, another downstream enzyme, the arachidonate monooxygenase CYP1B1, has been identified as a causative gene in primary congenital glaucoma (Vasiliou and Gonzalez, 2008).

Ocular hypertension is both a cause and consequence of compromised mechanotransduction that underlies the structural and functional changes associated with the decrease in conventional outflow resistance. Prospective randomized multicenter studies demonstrate that IOP reduction delays or even prevents the structural and functional damage of optic nerve axons in glaucoma (Kass et al., 2002; Leske et al., 2003) with an acceptable reduction in IOP by frontline drugs of ~20%. Given that compromised mechanotransduction may lead to increases in IOP and optic neuropathy by impairing TM filtering and regulation of aqueous outflow, delineation of the intrinsic molecular mechanisms provide new alternatives for treatment. Our findings predict that targeting TRPV4 and TREK-1 could be effective in modulating IOP; however, we also show that antihypertensive treatments will require careful consideration of interlocked signaling pathways that regulate calcium homeostasis, cytoskeletal dynamics, and pressure sensitivity in the TM.

Acknowledgments

This study was supported by the National Institutes of Health (R01EY022076, R01EY027920, T32EY024234, P30EY014800), Willard L. Eccles Charitable Foundation, Glaucoma Research Foundation, University of Utah Technology Acceleration Grant,

and an Unrestricted Grant from Research to Prevent Blindness to the Department of Ophthalmology at the University of Utah.

The authors declare no competing financial interests.

Author contributions: O. Yarishkin and D. Križaj designed research; O. Yarishkin, T.T.T. Phuong, C.A. Bretz, M. Lakk, J.M. Baumann, and K.W. Olsen performed research; O. Yarishkin, T.T.T. Phuong, M.E. Hartnett, and D. Križaj analyzed data; A. Crandall and C. Heurteaux provided tissue and reagents, O. Yarishkin and D. Križaj wrote the paper.

Sharon E. Gordon served as editor.

Submitted: 12 July 2018

Accepted: 26 October 2018

References

- Abad, E., G. Lorente, N. Gavara, M. Morales, A. Gual, and X. Gasull. 2008. Activation of store-operated Ca^{2+} channels in trabecular meshwork cells. *Invest. Ophthalmol. Vis. Sci.* 49:677–686. <https://doi.org/10.1167/iovs.07-1080>
- Acott, T.S., M.J. Kelley, K.E. Keller, J.A. Vranka, D.W. Abu-Hassan, X. Li, M. Aga, and J.M. Bradley. 2014. Intraocular pressure homeostasis: maintaining balance in a high-pressure environment. *J. Ocul. Pharmacol. Ther.* 30:94–101. <https://doi.org/10.1089/jop.2013.0185>
- Alloui, A., K. Zimmermann, J. Mamet, F. Duprat, J. Noël, J. Chemin, N. Guy, N. Blondeau, N. Voilley, C. Rubat-Coudert, et al. 2006. TREK-1, a K^+ channel involved in polymodal pain perception. *EMBO J.* 25:2368–2376. <https://doi.org/10.1038/sj.emboj.7601116>
- Anishkin, A., S.H. Loukin, J. Teng, and C. Kung. 2014. Feeling the hidden mechanical forces in lipid bilayer is an original sense. *Proc. Natl. Acad. Sci. USA.* 111:7898–7905. <https://doi.org/10.1073/pnas.1313364111>
- Baker, S.A., W.J. Hatton, J. Han, G.W. Hennig, F.C. Britton, and S.D. Koh. 2010. Role of TREK-1 potassium channel in bladder overactivity after partial bladder outlet obstruction in mouse. *J. Urol.* 183:793–800. <https://doi.org/10.1016/j.juro.2009.09.079>
- Bhatt, K., H. Gong, and T.F. Freddo. 1995. Freeze-fracture studies of interendothelial junctions in the angle of the human eye. *Invest. Ophthalmol. Vis. Sci.* 36:1379–1389.
- Bichet, D., S. Blin, S. Feliciangeli, F.C. Chatelain, N. Bobak, and F. Lesage. 2015. Silent but not dumb: how cellular trafficking and pore gating modulate expression of TWIK1 and THIK2. *Pflugers Arch.* 467:1121–1131. <https://doi.org/10.1007/s00424-014-1631-y>
- Bittner, S., T. Ruck, M.K. Schuhmann, A.M. Herrmann, H. Moha ou Maati, N. Bobak, K. Göbel, F. Langhauser, D. Stegner, P. Ehling, et al. 2013. Endothelial TWIK-related potassium channel-1 (TREK1) regulates immune-cell trafficking into the CNS. *Nat. Med.* 19:1161–1165. <https://doi.org/10.1038/nm.3303>
- Brohawn, S.G., Z. Su, and R. MacKinnon. 2014. Mechanosensitivity is mediated directly by the lipid membrane in TRAAK and TREK1 K^+ channels. *Proc. Natl. Acad. Sci. USA.* 111:3614–3619. <https://doi.org/10.1073/pnas.1320768111>
- Brubaker, R.F. 1975. The effect of intraocular pressure on conventional outflow resistance in the enucleated human eye. *Invest. Ophthalmol.* 14:286–292.
- Brubaker, R.F. 1991. Flow of aqueous humor in humans [The Friedenwald Lecture]. *Invest. Ophthalmol. Vis. Sci.* 32:3145–3166.
- Cadaveira-Mosquera, A., M. Pérez, A. Reboreda, P. Rivas-Ramírez, D. Fernández-Fernández, and J.A. Lamas. 2012. Expression of K2P channels in sensory and motor neurons of the autonomic nervous system. *J. Mol. Neurosci.* 48:86–96. <https://doi.org/10.1007/s12031-012-9780-y>
- Campbell, I.D., and M.J. Humphries. 2011. Integrin structure, activation, and interactions. *Cold Spring Harb. Perspect. Biol.* 3:a004994. <https://doi.org/10.1101/cshperspect.a004994>
- Carreon, T.A., A. Castellanos, X. Gasull, and S.K. Bhattacharya. 2017. Interaction of cochlin and mechanosensitive channel TREK-1 in trabecular meshwork cells influences the regulation of intraocular pressure. *Sci. Rep.* 7:452. <https://doi.org/10.1038/s41598-017-00430-2>
- Comes, N., X. Gasull, A. Gual, and T. Borrás. 2005. Differential expression of the human chloride channel genes in the trabecular meshwork under stress conditions. *Exp. Eye Res.* 80:801–813. <https://doi.org/10.1016/j.exer.2004.12.009>

- Decher, N., A.K. Kiper, and S. Rinné. 2017. Stretch-activated potassium currents in the heart: Focus on TREK-1 and arrhythmias. *Prog. Biophys. Mol. Biol.* 130:223–232.
- de la Peña, E., A. Mälikä, H. Vara, R. Caires, J.J. Ballesta, C. Belmonte, and F. Viana. 2012. The influence of cold temperature on cellular excitability of hippocampal networks. *PLoS One.* 7:e52475. <https://doi.org/10.1371/journal.pone.0052475>
- Dismuke, W.M., and D.Z. Ellis. 2009. Activation of the BK(Ca) channel increases outflow facility and decreases trabecular meshwork cell volume. *J. Ocul. Pharmacol. Ther.* 25:309–314. <https://doi.org/10.1089/jop.2008.0133>
- Downs, J.C. 2015. IOP telemetry in the nonhuman primate. *Exp. Eye Res.* 141:91–98. <https://doi.org/10.1016/j.exer.2015.07.015>
- Dyachenko, V., M. Zuzarte, C. Putzke, R. Preisig-Müller, G. Isenberg, and J. Daut. Xian Tao Li. 2006. The stretch-activated potassium channel TREK-1 in rat cardiac ventricular muscle. *Cardiovasc. Res.* 69:86–97. <https://doi.org/10.1016/j.cardiores.2005.08.018>
- Enyedi, P., and G. Czirják. 2010. Molecular background of leak K⁺ currents: two-pore domain potassium channels. *Physiol. Rev.* 90:559–605. <https://doi.org/10.1152/physrev.00029.2009>
- Feliciangeli, S., F.C. Chatelain, D. Bichet, and F. Lesage. 2015. The family of K2P channels: salient structural and functional properties. *J. Physiol.* 593:2587–2603. <https://doi.org/10.1113/jphysiol.2014.287268>
- Ferroni, S., P. Valente, M. Caprini, M. Nobile, P. Schubert, and C. Rapisarda. 2003. Arachidonic acid activates an open rectifier potassium channel in cultured rat cortical astrocytes. *J. Neurosci. Res.* 72:363–372. <https://doi.org/10.1002/jnr.10580>
- Fink, M., F. Duprat, F. Lesage, R. Reyes, G. Romey, C. Heurteaux, and M. Lazdunski. 1996. Cloning, functional expression and brain localization of a novel unconventional outward rectifier K⁺ channel. *EMBO J.* 15:6854–6862. <https://doi.org/10.1002/j.1460-2075.1996.tb10177.x>
- Flügel, C., E. Tamm, and E. Lütjen-Drecoll. 1991. Different cell populations in bovine trabecular meshwork: an ultrastructural and immunocytochemical study. *Exp. Eye Res.* 52:681–690. [https://doi.org/10.1016/0014-4835\(91\)90020-F](https://doi.org/10.1016/0014-4835(91)90020-F)
- Gasull, X., E. Ferrer, A. Llobet, A. Castellano, J.M. Nicolás, J. Palés, and A. Gual. 2003. Cell membrane stretch modulates the high-conductance Ca²⁺-activated K⁺ channel in bovine trabecular meshwork cells. *Invest. Ophthalmol. Vis. Sci.* 44:706–714. <https://doi.org/10.1167/iov.02-0384>
- Goel, M., A.E. Sienkiewicz, R. Picciani, J. Wang, R.K. Lee, and S.K. Bhattacharya. 2012. Cochlin, intraocular pressure regulation and mechanosensing. *PLoS One.* 7:e34309. <https://doi.org/10.1371/journal.pone.0034309>
- Grant, J., V. Tran, S.K. Bhattacharya, and L. Bianchi. 2013. Ionic currents of human trabecular meshwork cells from control and glaucoma subjects. *J. Membr. Biol.* 246:167–175. <https://doi.org/10.1007/s00232-012-9517-4>
- Gruss, M., T.J. Bushell, D.P. Bright, W.R. Lieb, A. Mathie, and N.P. Franks. 2004. Two-pore-domain K⁺ channels are a novel target for the anesthetic gases xenon, nitrous oxide, and cyclopropane. *Mol. Pharmacol.* 65:443–452. <https://doi.org/10.1124/mol.65.2.443>
- Heurteaux, C., N. Guy, C. Laigle, N. Blondeau, F. Duprat, M. Mazzuca, L. Lang-Lazdunski, C. Widmann, M. Zanzouri, G. Romey, and M. Lazdunski. 2004. TREK-1, a K⁺ channel involved in neuroprotection and general anesthesia. *EMBO J.* 23:2684–2695. <https://doi.org/10.1038/sj.emboj.7600234>
- Honoré, E. 2007. The neuronal background K2P channels: focus on TREK1. *Nat. Rev. Neurosci.* 8:251–261. <https://doi.org/10.1038/nrn2117>
- Honoré, E., F. Maingret, M. Lazdunski, and A.J. Patel. 2002. An intracellular proton sensor commands lipid- and mechano-gating of the K(+) channel TREK-1. *EMBO J.* 21:2968–2976. <https://doi.org/10.1093/emboj/cdf288>
- Jo, A.O., M. Lakk, A.M. Frye, T.T. Phuong, S.N. Redmon, R. Roberts, B.A. Berkowitz, O. Yarishkin, and D. Križaj. 2016. Differential volume regulation and calcium signaling in two ciliary body cell types is subserved by TRPV4 channels. *Proc. Natl. Acad. Sci. USA.* 113:3885–3890. <https://doi.org/10.1073/pnas.1515895113>
- Jo, A.O., J.M. Noel, M. Lakk, O. Yarishkin, D.A. Ryskamp, K. Shibasaki, M.A. McCall, and D. Križaj. 2017. Mouse retinal ganglion cell signalling is dynamically modulated through parallel anterograde activation of cannabinoid and vanilloid pathways. *J. Physiol.* 595:6499–6516. <https://doi.org/10.1113/jp274562>
- Kass, M.A., D.K. Heuer, E.J. Higginbotham, C.A. Johnson, J.L. Keltner, J.P. Miller, R.K. Parrish II, M.R. Wilson, and M.O. Gordon. 2002. The Ocular Hypertension Treatment Study: a randomized trial determines that topical ocular hypotensive medication delays or prevents the onset of primary open-angle glaucoma. *Arch. Ophthalmol.* 120:701–713, discussion: 829–830. <https://doi.org/10.1001/archophth.120.6.701>
- Kirber, M.T., R.W. Ordway, L.H. Clapp, J.V. Walsh Jr., and J.J. Singer. 1992. Both membrane stretch and fatty acids directly activate large conductance Ca(2+)-activated K+ channels in vascular smooth muscle cells. *FEBS Lett.* 297:24–28. [https://doi.org/10.1016/0014-5793\(92\)80319-C](https://doi.org/10.1016/0014-5793(92)80319-C)
- Lakk, M., O. Yarishkin, J.M. Baumann, A. Iuso, and D. Križaj. 2017. Cholesterol regulates polymodal sensory transduction in Müller glia. *Glia.* 65:2038–2050. <https://doi.org/10.1002/glia.23213>
- Last, J.A., T. Pan, Y. Ding, C.M. Reilly, K. Keller, T.S. Acott, M.P. Fautsch, C.J. Murphy, and P. Russell. 2011. Elastic modulus determination of normal and glaucomatous human trabecular meshwork. *Invest. Ophthalmol. Vis. Sci.* 52:2147–2152. <https://doi.org/10.1167/iov.10-6342>
- Lei, Q., X.Q. Pan, S. Chang, S.B. Malkowicz, T.J. Guzzo, and A.P. Malykhina. 2014. Response of the human detrusor to stretch is regulated by TREK-1, a two-pore-domain (K2P) mechano-gated potassium channel. *J. Physiol.* 592:3013–3030. <https://doi.org/10.1113/jphysiol.2014.271718>
- Lei, Y., D.R. Overby, A. Boussemier-Calleja, W.D. Stamer, and C.R. Ethier. 2011. Outflow physiology of the mouse eye: pressure dependence and washout. *Invest. Ophthalmol. Vis. Sci.* 52:1865–1871. <https://doi.org/10.1167/iov.10-6019>
- Lembrechts, R., I. Pintelon, K. Schnorbusch, J.P. Timmermans, D. Adriaensen, and I. Brouns. 2011. Expression of mechanogated two-pore domain potassium channels in mouse lungs: special reference to mechanosensory airway receptors. *Histochem. Cell Biol.* 136:371–385. <https://doi.org/10.1007/s00418-011-0837-8>
- Lepple-Wienhues, A., F. Stahl, U. Willner, R. Schäfer, and M. Wiederholt. 1991. Endothelin-evoked contractions in bovine ciliary muscle and trabecular meshwork: interaction with calcium, nifedipine and nickel. *Curr. Eye Res.* 10:983–989. <https://doi.org/10.3109/02713689109020335>
- Lepple-Wienhues, A., R. Rauch, A.F. Clark, A. Grässmann, S. Berweck, and M. Wiederholt. 1994. Electrophysiological properties of cultured human trabecular meshwork cells. *Exp. Eye Res.* 59:305–311. <https://doi.org/10.1006/exer.1994.1112>
- Lesage, F., and M. Lazdunski. 2000. Molecular and functional properties of two-pore-domain potassium channels. *Am. J. Physiol. Renal Physiol.* 279:F793–F801. <https://doi.org/10.1152/ajprenal.2000.279.5.F793>
- Leske, M.C., A. Heijl, M. Hussein, B. Bengtsson, L. Hyman, and E. Komaroff. Early Manifest Glaucoma Trial Group. 2003. Factors for glaucoma progression and the effect of treatment: the early manifest glaucoma trial. *Arch. Ophthalmol.* 121:48–56. <https://doi.org/10.1001/archophth.121.1.48>
- Liu, H., J.A. Enyeart, and J.J. Enyeart. 2007. Potent inhibition of native TREK-1 K⁺ channels by selected dihydropyridine Ca²⁺ channel antagonists. *J. Pharmacol. Exp. Ther.* 323:39–48. <https://doi.org/10.1124/jpet.107.125245>
- Llobet, A., X. Gasull, J. Palés, E. Martí, and A. Gual. 2001. Identification of Kir2.1 channel activity in cultured trabecular meshwork cells. *Invest. Ophthalmol. Vis. Sci.* 42:2371–2379.
- Lolicato, M., C. Arrigoni, T. Mori, Y. Sekioka, C. Bryant, K.A. Clark, and D.L. Minor Jr. 2017. K_{2P}2.1 (TREK-1)-activator complexes reveal a cryptic selectivity filter binding site. *Nature.* 547:364–368. <https://doi.org/10.1038/nature22988>
- Lütjen-Drecoll, E., and J.W. Rohen. 1989. Morphology of aqueous outflow pathways in normal and glaucomatous eyes. In *The Glaucomas*. E.A. Klein, editor. Mosby, St Louis. 89–123.
- Maingret, F., A.J. Patel, F. Lesage, M. Lazdunski, and E. Honoré. 1999. Mechano- or acid stimulation, two interactive modes of activation of the TREK-1 potassium channel. *J. Biol. Chem.* 274:26691–26696. <https://doi.org/10.1074/jbc.274.38.26691>
- Maingret, F., E. Honoré, M. Lazdunski, and A.J. Patel. 2002. Molecular basis of the voltage-dependent gating of TREK-1, a mechano-sensitive K(+) channel. *Biochem. Biophys. Res. Commun.* 292:339–346. <https://doi.org/10.1006/bbrc.2002.6674>
- Mazella, J., O. Pétrault, G. Lucas, E. Deval, S. Béraud-Dufour, C. Gandin, M. El-Yacoubi, C. Widmann, A. Guyon, E. Chevet, et al. 2010. Spadin, a sortilin-derived peptide, targeting rodent TREK-1 channels: a new concept in the antidepressant drug design. *PLoS Biol.* 8:e1000355. <https://doi.org/10.1371/journal.pbio.1000355>
- Meadows, H.J., C.D. Benham, W. Cairns, I. Gloger, C. Jennings, A.D. Medhurst, P. Murdock, and C.G. Chapman. 2000. Cloning, localisation and functional expression of the human orthologue of the TREK-1 potassium channel. *Pflugers Arch.* 439:714–722. <https://doi.org/10.1007/s004249900235>
- Meves, H. 2008. Arachidonic acid and ion channels: an update. *Br. J. Pharmacol.* 155:4–16. <https://doi.org/10.1038/bjp.2008.216>
- Mitchell, C.H., J.C. Fleischhauer, W.D. Stamer, K. Peterson-Yantorno, and M.M. Civan. 2002. Human trabecular meshwork cell volume regula-

- tion. *Am. J. Physiol. Cell Physiol.* 283:C315–C326. <https://doi.org/10.1152/ajpcell.00544.2001>
- Molnár, T., O. Yarishkin, A. Iuso, P. Barabas, B. Jones, R.E. Marc, T.T. Phuong, and D. Križaj. 2016. Store-operated calcium entry in Müller glia is controlled by synergistic activation of TRPC and Orai channels. *J. Neurosci.* 36:3184–3198. <https://doi.org/10.1523/JNEUROSCI.4069-15.2016>
- Monaghan, K., S.A. Baker, L. Dwyer, W.C. Hatton, K. Sik Park, K.M. Sanders, and S.D. Koh. 2011. The stretch-dependent potassium channel TREK-1 and its function in murine myometrium. *J. Physiol.* 589:1221–1233. <https://doi.org/10.1113/jphysiol.2010.203869>
- Nayak, T.K., S. Harinath, S. Nama, K. Somasundaram, and S.K. Sikdar. 2009. Inhibition of human two-pore domain K⁺ channel TREK1 by local anesthetic lidocaine: negative cooperativity and half-of-sites saturation kinetics. *Mol. Pharmacol.* 76:903–917. <https://doi.org/10.1124/mol.109.056838>
- Noël, J., G. Sandoz, and F. Lesage. 2011. Molecular regulations governing TREK and TRAAK channel functions. *Channels (Austin)*. 5:402–409. <https://doi.org/10.4161/chan.5.5.16469>
- Patel, A.J., E. Honoré, F. Maingret, F. Lesage, M. Fink, F. Duprat, and M. Lazdunski. 1998. A mammalian two pore domain mechano-gated S-like K⁺ channel. *EMBO J.* 17:4283–4290. <https://doi.org/10.1093/emboj/17.15.4283>
- Patel, A.J., E. Honoré, F. Lesage, M. Fink, G. Romey, and M. Lazdunski. 1999. Inhalational anesthetics activate two-pore-domain background K⁺ channels. *Nat. Neurosci.* 2:422–426. <https://doi.org/10.1038/8084>
- Pattabiraman, P.P., R. Maddala, and P.V. Rao. 2014. Regulation of plasticity and fibrogenic activity of trabecular meshwork cells by Rho GTPase signaling. *J. Cell. Physiol.* 229:927–942. <https://doi.org/10.1002/jcp.24524>
- Phuong, T.T.T., S.N. Redmon, O. Yarishkin, J.M. Winter, D.Y. Li, and D. Križaj. 2017. Calcium influx through TRPV4 channels modulates the adherens contacts between retinal microvascular endothelial cells. *J. Physiol.* 595:6869–6885. <https://doi.org/10.1113/JP275052>
- Qiu, Y., R. Liao, and X. Zhang. 2008. Real-time monitoring primary cardiomyocyte adhesion based on electrochemical impedance spectroscopy and electrical cell-substrate impedance sensing. *Anal. Chem.* 80:990–996. <https://doi.org/10.1021/ac701745c>
- Ramachandran, C., R.V. Patil, K. Combrink, N.A. Sharif, and S.P. Srinivas. 2011. Rho-Rho kinase pathway in the actomyosin contraction and cell-matrix adhesion in immortalized human trabecular meshwork cells. *Mol. Vis.* 17:1877–1890.
- Reyes, R., F. Duprat, F. Lesage, M. Fink, M. Salinas, N. Farman, and M. Lazdunski. 1998. Cloning and expression of a novel pH-sensitive two pore domain K⁺ channel from human kidney. *J. Biol. Chem.* 273:30863–30869. <https://doi.org/10.1074/jbc.273.47.30863>
- Ryskamp, D.A., A.O. Jo, A.M. Frye, F. Vazquez-Chona, N. MacAulay, W.B. Thoreson, and D. Križaj. 2014. Swelling and eicosanoid metabolites differentially gate TRPV4 channels in retinal neurons and glia. *J. Neurosci.* 34:15689–15700. <https://doi.org/10.1523/JNEUROSCI.2540-14.2014>
- Ryskamp, D.A., A. Iuso, and D. Križaj. 2015. TRPV4 links inflammatory signaling and neuroglial swelling. *Channels (Austin)*. 9:70–72. <https://doi.org/10.1080/19336950.2015.1017998>
- Ryskamp, D.A., A.M. Frye, T.T.T. Phuong, O. Yarishkin, A.O. Jo, Y. Xu, M. Lakk, A. Iuso, S.N. Redmon, B. Ambati, et al. 2016. TRPV4 regulates calcium homeostasis, cytoskeletal remodeling, conventional outflow and intraocular pressure in the mammalian eye. *Sci. Rep.* 6:30583. <https://doi.org/10.1038/srep30583>
- Sachs, F. 2010. Stretch-activated ion channels: what are they? *Physiology (Bethesda)*. 25:50–56.
- Stamer, W.D., and A.F. Clark. 2017. The many faces of the trabecular meshwork cell. *Exp. Eye Res.* 158:112–123. <https://doi.org/10.1016/j.exer.2016.07.009>
- Talley, E.M., G. Solorzano, Q. Lei, D. Kim, and D.A. Bayliss. 2001. Cns distribution of members of the two-pore-domain (KCNK) potassium channel family. *J. Neurosci.* 21:7491–7505. <https://doi.org/10.1523/JNEUROSCI.21-19-07491.2001>
- Thompson, J.L., and T.J. Shuttleworth. 2013. Molecular basis of activation of the arachidonate-regulated Ca²⁺ (ARC) channel, a store-independent Orai channel, by plasma membrane STIM1. *J. Physiol.* 591:3507–3523. <https://doi.org/10.1113/jphysiol.2013.256784>
- Toft-Bertelsen, T.L., D. Križaj, and N. MacAulay. 2017. When size matters: transient receptor potential vanilloid 4 channel as a volume-sensor rather than an osmo-sensor. *J. Physiol.* 595:3287–3302. <https://doi.org/10.1113/JP274135>
- Torreon, K.Y., E.L. Papke, J.R. Halman, J. Stolwijk, C.N. Dautriche, M. Bergkvist, J. Danias, S.T. Sharfstein, and Y. Xie. 2016. Bioengineered glaucomatous 3D human trabecular meshwork as an in vitro disease model. *Biotechnol. Bioeng.* 113:1357–1368. <https://doi.org/10.1002/bit.25899>
- Tran, V.T., P.T. Ho, L. Cabrera, J.E. Torres, and S.K. Bhattacharya. 2014. Mechanotransduction channels of the trabecular meshwork. *Curr. Eye Res.* 39:291–303. <https://doi.org/10.3109/02713683.2013.842593>
- Vasilio, V., and F.J. Gonzalez. 2008. Role of CYP1B1 in glaucoma. *Annu. Rev. Pharmacol. Toxicol.* 48:333–358. <https://doi.org/10.1146/annurev-pharmtox.48.061807.154729>
- Wang, H., X. Han, C.A. Bretz, S. Becker, D. Gambhir, G.W. Smith, R.J. Samulski, E.S. Wittchen, L.A. Quilliam, M. Chrzanowska-Wodnicka, and M.E. Hartnett. 2016. Retinal pigment epithelial cell expression of active Rap1a by scAAV2 inhibits choroidal neovascularization. *Mol. Ther. Methods Clin. Dev.* 3:16056. <https://doi.org/10.1038/mtm.2016.56>
- Weinreb, R.N., J.R. Polansky, J.A. Alvarado, and M.D. Mitchell. 1988. Arachidonic acid metabolism in human trabecular meshwork cells. *Invest. Ophthalmol. Vis. Sci.* 29:1708–1712.
- White, J.P., M. Cibelli, L. Urban, B. Nilius, J.G. McGeown, and I. Nagy. 2016. TRPV4: Molecular Conductor of a Diverse Orchestra. *Physiol. Rev.* 96:911–973. <https://doi.org/10.1152/physrev.00016.2015>
- Wiederholt, M., H. Thieme, and F. Stumpff. 2000. The regulation of trabecular meshwork and ciliary muscle contractility. *Prog. Retin. Eye Res.* 19:271–295. [https://doi.org/10.1016/S1350-9462\(99\)00015-4](https://doi.org/10.1016/S1350-9462(99)00015-4)
- Yarishkin, O., T.T.T. Phuong, J.M. Baumann, A.S. Crandall, F. Ahmed, K. Torreon, and D. Križaj. 2018. Tandem-pore domain potassium channels are components of intracellular signaling pathways, determinants of pH sensitivity and mechanosensitivity of human trabecular meshwork cells. *Invest. Ophthalmol. Vis. Sci.* 59:1660.